Politecnico di Torino

Master of Science in Geoenergy and Georesources Engineering

Flow Dynamic Simulation of CO2 Injection In Underground Porous Media

Supervisors:
Prof. Dario Viberti
Eloisa Salina Borello

Candidate:
Shahab Angali

Abstract

Carbon dioxide (CO2) trapping in capillary networks of reservoir rocks is a pathway to long term geological storage. At pore scale, the CO2 trapping potential depends on injection pressure, temperature, and the rock's interaction with the surrounding fluids. Modeling this interaction requires adequate representations of both capillary volume and surface. For the lack of scalable representations, however, the prediction of a rock's CO2 storage potential has been challenging.[2]

In this thesis we start with CCS (carbon capture and storage) technologies,different types of storage, and CO_2 trapping mechanisms, in the following we build 3D reservoir model and doing simulation using two different softwares, Open Porous Media (OPM) and tNavigator, to evaluate the effect of critical reservoir properties and operational parameters. These include depth, permeability, critical gas saturation, injection rates, and pressure constrain.

In the second part we do sensitivity analysis to analyse the influence of these parameters on CO_2 behavior and storage performance. Additionally, the study explores the influence of convective dissolution and diffusion in brine systems, in the result we can see while dissolution plays a significant role in CO_2 distribution and pressure profile, diffusion has minimum effect under modeled conditions.

Finally, we comapre the results from OPM and tNavigator, which show the high similarity in result such as gas saturation, well pressure, and total gas injection, tNavigator offering enhanced compositional modeling capabilities.

This study provid a good overview for operational strategies for future CCS projects, which is useful for reducing atmospheric CO_2 and removing the impacts of climate change.

Table of Contents

Scope of Work 8
I. Introduction 9
1. Carbon Capture and Storage 11
2. Physical properties that influence CO2 injection 12
3. Underground storage types 13
4. Trapping mechanisms 15
5. Underground CO2 behavior 18
6. Numerical simulation and modeling 21
7. Objectives of the thesis 21
II. Models' description 22
1. Rock fluid parameters 23
2. Simulation with Open Porous Media software (OPM) 23
III. Simulation Result 25
1. Convective Dissolution 27
2. Sensitivity analysis 30
2.1. Block Gas Saturation: 30
2.2. Well Bottomhole Pressure (WBHP) and Well Bottom Pressure (WBP): 31
2.3. Total Gas Injection (WGIT) and Gas Injection Rate (WGIR): 33
2.4. Field Gas In Place (FGIP): 34
IV. Comparison of CO_2 Injection Modeling via CO2STORE in OPM vs. tNavigator 35
1. CO2STORE in OPM 35
2. CO2STORE in tNavigator 36
3. Comparison of Block Gas Saturation in Tnavigator and OPM 39
4. Comparison of WBHP and WBP in tNavigator and OPM 40
5. Comparison of WGIT and WGIR in tNavigator and OPM: 40
6. Comparison of FGIP in TNavigator and OPM: 41
7. Changing Kr exponent in OPM: 42
8. Dissolution (DISS) vs. Diffusion (DIFF) in CO_2–Brine Systems in OPM: 45
V. Conclusion 48
Appendix A: Input File of base model in OPM 49
Appendix B: Input File of base model in tNavigator 51
BIBLIOGRAPHY 54

List of Figures

Figure 1 The percentages of CO2 emissions from different sectors (Main sources of carbon dioxide emissions, n.d.). [5] 9
Figure 2 Illustration of global CO2 emissions from energy sources in 2000 and 2021 [6] 10
Figure 3 Global CO2 emissions and atomespheric CO2 . [7] 10
Figure 5 scheme of the different uses of captured CO2 [11] 12
Figure 6 CCS storage types[15] 14
Figure 7 Unconfined and confined saline aquifers [19] 15
Figure 8 CO2 trapping mechanisms and storage security [22] 16
Figure 9 Impact of faults on plume migration in a CO2 storage site [1] 16
Figure 10 Residual trapping of CO2 [13] 17
Figure 11 CO2 trapping within a reservoir on a microscopic scale[25] 18
Figure 12 CO2 phase diagram.[27] 19
Figure 13 Supercritical carbon dioxide density as a function of the pressure and temperature [28] 20
Figure 14 CO2 concentration in different pressures and temperatures [29] 20
Figure 15 3D representation of reservoir model. 22
Figure 16 The location of the injection well. 26
Figure 17 The location of monitoring grid blocks 26
Figure 18 Field Gas Injection total(FGIT m3) vs date for different DRST values with WBHP=300bar 28
Figure 19 Field Average Pressure vs date for different DRST values with WBHP=300bar 28
Figure 20 Field Gas Injection total(FGIT m3) vs date for different DRST values with WBHP=250bar 29
Figure 21 Field Average Pressure vs date for different DRST values with WBHP=250bar 29
Figure 22 Block gas saturation vs Time for upper block (1,11,1) 31
Figure 23 Block gas saturation vs Time for middle block (1,11,10) 31
Figure 24 Block gas saturation vs Time for lower block (1,11,20) 31
Figure 25 well bottom hole pressure (WBHP-left plot) and well bottom pressure (WBP-right plot) vs Date. 32
Figure 26 Total gas injection (WGIT) in Sm^3 vs Date for Sgc=0 and Sgc=.015 33
Figure 27 Gas injection rate (WGIR) in Sm^3/day vs Date for Sgc=0 and Sgc=.015 33
Figure 28 Field Gas In Place (FGIP) in Sm^3 vs Date for Sgc=0 and Sgc=.015 34
Figure 29 Block gas saturation vs Time for upper block (1,11,1) 39
Figure 30 Block gas saturation vs Time for middle block (1,11,1) 39
Figure 31 Block gas saturation vs Time for lower block (1,11,20) 40
Figure 32 well bottom hole pressure (WBHP-left plot) and well bottom pressure (WBP-right plot) vs Date. 40
Figure 33 Gas injection rate (WGIR) in Sm^3/day vs Date in Tnav (blue) and OPM (red) 41
Figure 34 Total gas injection (WGIT) in Sm^3 vs Date in Tnav (blue) and OPM (red) 41
Figure 35 Field Gas In Place (FGIP) in Sm^3 vs Date for tNav and OPM 42
Figure 36 Block gas saturation vs Time for upper block (1,11,1) for ng=no=2 and base case. 44
Figure 37 Block gas saturation vs Time for middle block (1,11,10) for ng=no=2 and base case. 44
Figure 38 Block gas saturation vs Time for lower block (1,11,20) for ng=no=2 and base case. 45
Figure 39 Block gas saturation vs Time for upper and lower block in dissolution and diffusion 45
Figure 40 Well bottom hole pressure vs Time in dissolution and diffusion 46
Figure 41 Well gas injection rate vs Time in dissolution and diffusion 46
Figure 42 Well gas injection total vs Time in dissolution and diffusion 47
Figure 43 Field gas in place vs Time in dissolution and diffusion 47

List of tables

Table 1 Storage capacity for several geological storage options [23] 15
Table 2 CO2 supercritical phase conditions 19
Table 3 Average parameters value..... 23
Table 4 Average parameters value..... 30
Table 5 CO_2–brine properties references in OPM [42]..... 36
Table 6 Compare CO2STORE keyword features in OPM and tNavigator 38

Nomenclature list

Symbol	Description
φ	Porosity
A_α	Accumulation term for phase α (e.g., water, oil, gas, solvent)
u_α	Velocity of component α
Q_α	well out flux density of pseudo component α , (negative for well in-flow)
b_α	shrinkage/expansion factor for phase α
S_α	Saturation of phase α
v_α	Velocity of phase α, based on Darcy's law
K	Permeability of the porous medium.
p_α	Pressure of phase α
$\bar{\rho_\alpha}$	Density of phase α
g	Gravitational acceleration vector
$\mu_{\alpha e}$	Effective viscosity of phase α
k_{rae}	Effective relative permeability of phase α
M	Miscibility interpolation factor (0: immiscible, 1: miscible)
r_v	Oil-gas ratio or condensate-gas ratio
r_s	Gas-oil ratio ("GOR")
ω	Todd-Longstaff mixing parameter
K_{ro}	Relative permeability to oil
K_{rw}	Relative permeability to water
n_o	Corey oil exponent
n_w	Corey water exponent
S_{wcr}	Critical water saturation

Scope of Work

This thesis focuses on evaluating the feasibility, effectiveness, and long-term performance of carbon dioxide (CO_2) storage in underground porous media, with particular emphasis on depleted gas reservoirs and deep saline aquifers—two of the most promising geological formations for large-scale CO_2 trapping. These underground formations can hold large amounts of CO_2 and, if well understood and managed, can keep it safely stored for a long time. This research mainly aims to understand how different geological, petrophysical, and operational factors affect key elements of the storage process—such as how much CO_2 can be stored, how effectively it can be injected, how pressure is managed, and how CO_2 moves through the reservoir over time. This study uses software simulation tools to model how CO_2 and brine behave underground, including how they interact during storage. By creating a base model of reservoir we try in this thesis to know what parameters affect on CO_2 injection in underground reservoir.

The scope of the study includes:

- **Review of CCS**: An overview of Carbon Capture and Storage (CCS) technologies,and different storage mechanisms, different types of geological formations, and the physical and chemical behavior of CO_2 in reservoir condition.
- **Create Reservoir Model**: we create 3D reservoir model in a saline aquifer. The model includes reservoir and fluid properties such as porosity, permeability, temperature, and salinity.
- **Simulation Tools**: Using of two simulation softwares ,Open Porous Media (OPM) and tNavigator, for simulation of CO_2 injection and storage and then we compare the results of these simulators with eachother.
- **Sensitivity Analysis**: Sensitivity of key factors, including reservoir depth, permeability, residual gas saturation, maximum gas relative permeability and convective dissolution and compare the result with different values of each.
- **Evaluation of Dissolution and Diffusion**: Analysis the effects of dissolution and diffusion of CO_2 into brine,and compare the result in terms of total injectivity.
- **Simulator Comparison**: comparison of OPM and tNavigator outputs in the same conditions to see the performance in simulation CO_2 injection process.

By discussing the upper part we want to evalute the best condition for CO_2 storage, this goal gained from the sensitivity analyses, simulation comparisons, and modeling of dissolution and diffusion processes.In the end, this research helps to make better decisions for using CCS technologies on a large scale to fight climate change.

I. Introduction

In recent years, climate change has become a critical global issue. Many of the environmental changes previously predicted by scientists are now taking place, including the melting of polar ice sheets, rising sea levels, more frequent heatwaves, and an overall increase in global temperatures. The primary driver behind these changes is well understood: the release of greenhouse gases into the atmosphere.

The greenhouse effect itself occurs when short-wave solar radiation (which is not impeded by the greenhouse gases) heats the surface of the Earth, and the energy is radiated back through the Earth's atmosphere as heat, with a longer wavelength. In the wavelengths 5-30 µm a lot of this thermal radiation is absorbed by water vapour and carbon dioxide, which in turn radiate it, thus heating the atmosphere and land and ocean surface. This is natural and what keeps the Earth habitable. Without the greenhouse effect overnight temperatures would plunge and the average surface temperature would be about minus 18 °C, about the same as on the moon, which lacks the shroud of our atmosphere. We owe the difference of some 33 °C substantially to natural levels of water vapour (60%, or more including clouds) and carbon dioxide in the Earth's atmosphere.[3]

Human activities such as the burning of oil, coal and gas, as well as deforestation are the primary cause of the increased carbon dioxide concentrations in the atmosphere. As shown in the Figure 1, 87% of all human-produced CO2 emissions come from the burning of fossil fuels like coal, natural gas and oil. The remainder results from the clearing of forests and other land use changes (9%), as well as some industrial processes such as cement manufacturing (4%).[4]

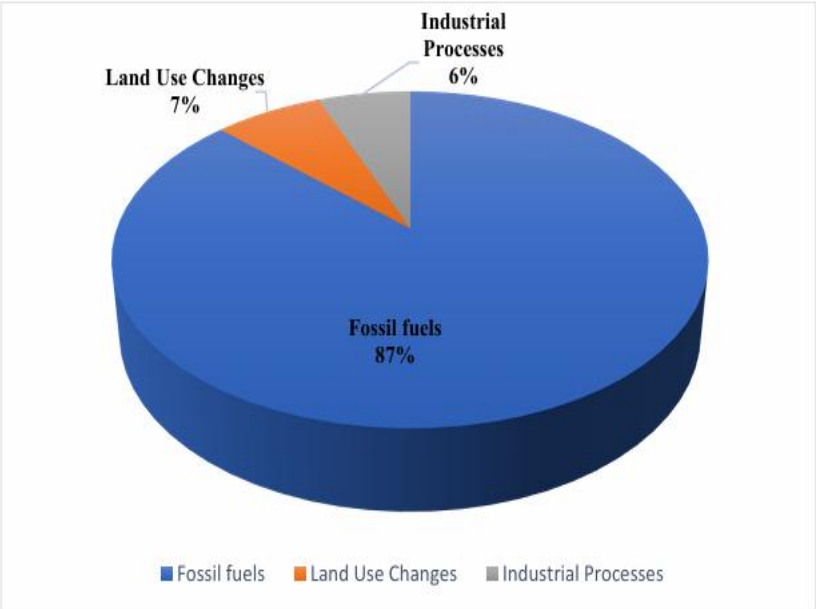

Figure 1 The percentages of CO2 emissions from different sectors (Main sources of carbon dioxide emissions, n.d.). [5]

The comparison of the emissions from the different energy sectors in the years 2000 and 2021 is shown in Figure 2. In comparison to the other energy sectors—natural gas, crude oil, and biomass, coal has the highest emissions in both of the years. Over the previous 20 years, coal emissions have doubled to a total of 15 Gt CO2. As it can be seen from the Figure 2., in both 2000 and 2021, energy combustion and industrial operations are the primary sources of CO2 emissions into the environment.[6]

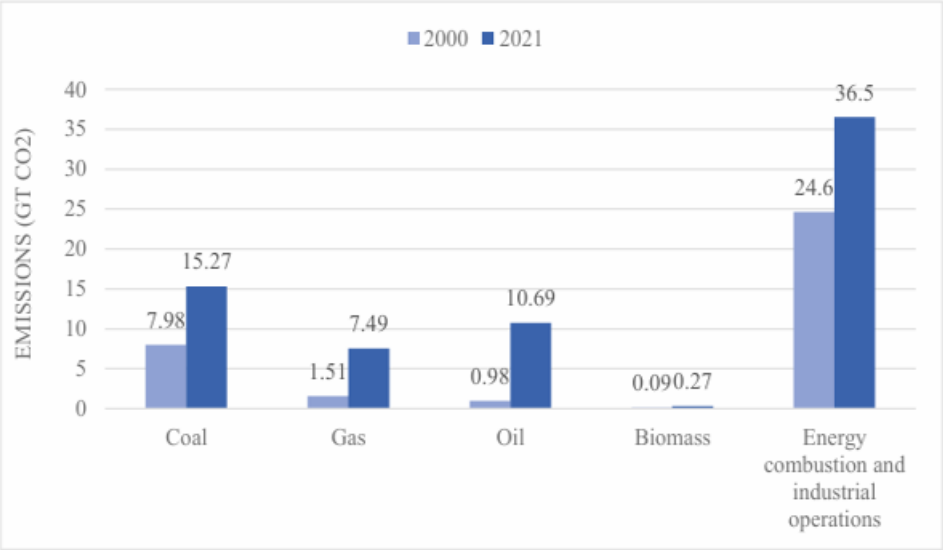

Figure 2 Illustration of global CO2 emissions from energy sources in 2000 and 2021 [6]

Nowadays, annual emissions of carbon dioxide from burning fossil fuels have increased every decade, from close to 11 billion tons of carbon dioxide per year in the 1960s to an estimated 37.4 billion tons in 2024.[7]

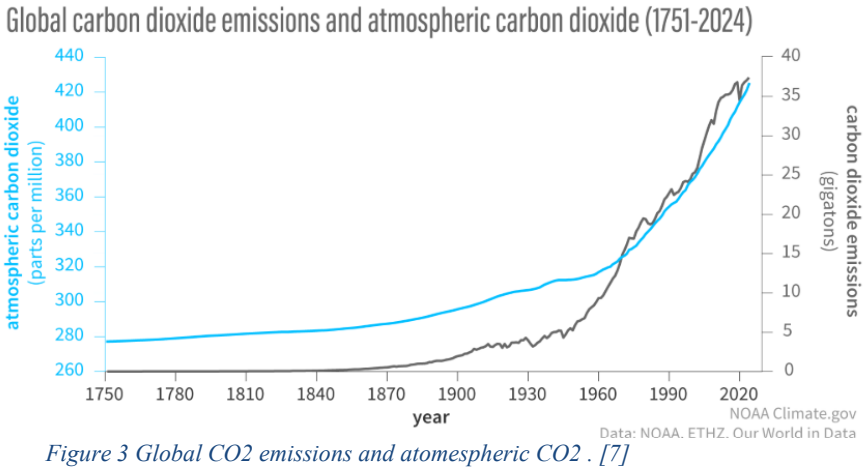

Figure 3 Global CO2 emissions and atomespheric CO2 . [7]

If global energy demand continues to rise fast predominantly fueled with fossil fuels, human emissions of carbon dioxide might reach 75 billion tons per year or more by the end of this century [8].

The Paris Agreement is a legally binding international treaty on climate change. It was adopted by 195 Parties at the UN Climate Change Conference (COP21) in Paris, France, on 12 December 2015. It entered into force on 4 November 2016. Its overarching goal is to hold "the increase in the global average temperature to well below 2°C above pre-industrial levels" and pursue efforts "to limit the temperature increase to 1.5°C above pre-industrial levels."

However, in recent years, world leaders have stressed the need to limit global warming to 1.5°C by the end of this century. That's because the UN's Intergovernmental Panel on Climate Change indicates that crossing the 1.5°C threshold risks unleashing far more severe climate change impacts, including more frequent and severe droughts, heatwaves and rainfall. To limit global warming to 1.5°C, greenhouse gas emissions must peak before 2025 at the latest and decline 43% by 2030.[9]

The Paris Agreement is a landmark in the multilateral climate change process because, for the first time, a binding agreement brings all nations together to combat climate change and adapt to its effects.

A net-zero energy system requires an important change in how we consume and generate energy, that we can access with different types of technologies.

Carbon capture, utilization, and storage (CCUS) is one of the few technologies that helping reduce emissions from different industries and remove CO_2 from the atmosphere. This is an important tool for reaching "net zero" goals, especially for emissions.

1. Carbon Capture and Storage

Carbon capture and storage (CCS) technologies were introduced following the agreement made in July 2009 by 17 members of the Major Economies Forum (MEF) on Energy and Climate. This initiative aimed to facilitate a transition to a low-carbon economy, supporting economic growth while addressing climate change. These technologies are able to capturing over 90% of CO2 emissions, mainly generated by fossil fuel combustion during industrial operations and electricity production. Once captured, the CO2 is transported—via pipelines, ships, or road tankers—and securely stored underground in depleted oil and gas reservoirs or deep saline aquifers situated a few kilometers below the Earth's surface .

In addition carbon capture utilization (CCU) is another approach that can work alongside or instead of carbon capture and storage (CCS). In CCU, the captured CO_2 is turned into different products using chemical, biological, light-based, or electrical reactions. These products include things like urea, polymers, and carbonates, or fuels such as syngas and methane.

However, one of the main issues with CCU is that the CO_2 used in these products is not stored permanently. Most of it eventually returns to the atmosphere, which limits how much CCU can help with fighting climate change. Because of this, CCU alone isn't enough to reduce emissions in the long term. To make it more effective, a permanent storage method—like using CO_2 in Enhanced Oil Recovery (EOR)—needs to be include.[10]

EOR is a family of techniques, some of them involving injecting CO2 into depleted oil fields. Several large-scale EOR projects in Norway, Canada, and Algeria have successfully stored 1 to 3 million metric tons of CO2 annually over several years, offering useful evidence to show that geological CCS is a reliable option . In the United States, which accounts for 94% of global CO2/EOR production, approximately 63 million metric tons of CO2—mainly from natural sources—are injected annually for this purpose.

The various potential applications of CO2 are summarized in the following diagram (Fig. 5).

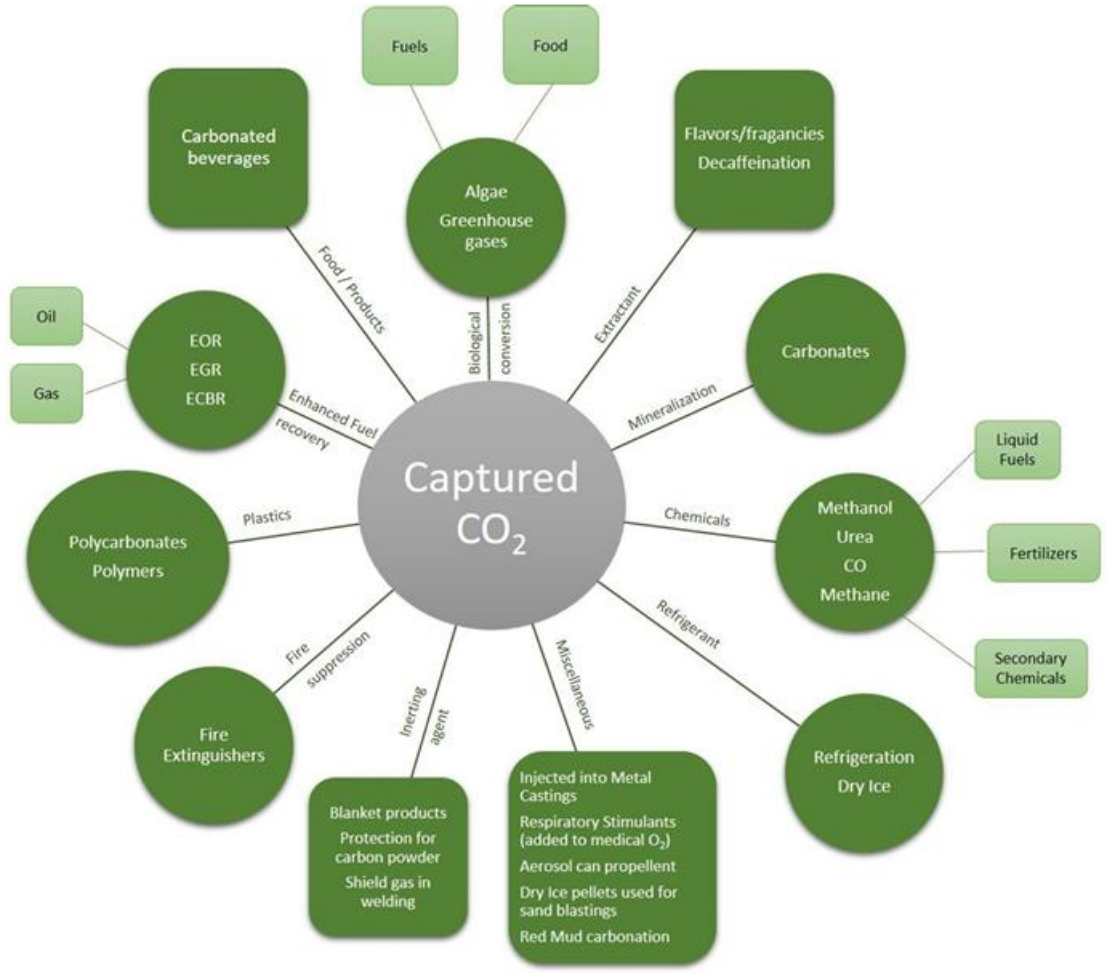

Figure 4 scheme of the different uses of captured CO2 [11]

Currently, CCU technologies utilize approximately 115 million tons of CO2 per year globally, which is minimal compared to the over 30 billion metric tons of CO2 emitted worldwide annually. Despite this, the recycling and conversion of CO2 into chemicals are anticipated to grow, increasing from around 0.5% of current carbon dioxide emissions to an estimated 1–2% in the future.[12]

2. Physical properties that influence CO2 injection

Three physical properties – permeability, pressure and porosity – influence how much CO2 can be injected into a reservoir, at what rate and for how long.

Permeability describes the way which fluids can move through rock formations it means how hard or easy for fluid to flow in the porous media. Although it is related to porosity, the permeability more depends on the shape of the grains and connectivity of the pore spaces. We can measure the permeablity from direct method or during well testing procedures. Additionally, when we have two or more fluids in the porous media, the relative permeability becomes important , it is related to ablity to flow of different fluid in the reservoir compared to

eachother and can be measured in a lab, modelled using simulations or calculated from field data.

Pressure controls how easily CO2 can be injected and how much CO2 can be safely stored. Reservoir pressure is the pressure of fluid within the pores of the reservoir. It can be measured using bottom-hole pressure gauges and during well tests. Reservoir pressure changes with subsurface activity. Extraction removes fluids and usually causes pressure to decrease. Injection adds fluids and usually causes pressure to increase. Fracture pressure is the pressure required to fracture a reservoir or its seal.

Porosity is the volume of rock pores as a proportion of the total rock volume. Porosity can be measured directly from core samples or it can be derived during well logging – the process of recording the geological and geophysical characteristics of a well.

CO2 is injected into a reservoir via a well at a pressure higher than that of the fluids within the target rock formation. Once CO2 is injected, it forms a plume that migrates through the reservoir, pushing pre-existing reservoir fluids away from the injection zone. The CO2 migrates within a network of interconnected pores where it mixes with or displaces pre-existing reservoir fluids. Fluid displacement and CO2 injection cause pressure to build within the reservoir. Elevated pressure from around the injection zone will disperse through the reservoir and potentially into surrounding rock formations, travelling faster and further than the CO2 plume or displaced fluids. In certain cases, increased subsurface pressure might be observed more than 100 km from the injection zone. Pressure increase is an expected part of large-scale operations, and different techniques have been developed to manage it.

The volume of CO2 that can be stored is determined by the pressure limits of a reservoir and how reservoir pressure responds to injection, as influenced by its porosity and permeability. A high quality reservoir can have a porosity of 25% or more, be very permeable and be at or below its natural hydrostatic pressure.[13] In addition, caprock plays a critical role in subsurface reservoir systems by providing a seal that prevents the upward migration of fluids. Typically composed of fine-grained, low-permeability materials like shale, salt, or anhydrite, caprock must possess sufficient thickness, mechanical integrity, and continuity to effectively contain hydrocarbons or injected substances such as CO_2.

3. Underground storage types

Following the CO2 absorption process is complete, we need to store it so that it is not released into the atmosphere. One of the best ways to store it is in underground reservoirs , which is the subject of much research..

The main geological storage options are: oil and gas reservoirs, deep saline aquifers, coal beds, caverns and mines.

An important challenge is the estimation of the capacity of geological storage. A major contribution towards the storage potential in Europe was the EU supported GESTCO study. Based on this study the storage capacity is not a limiting factor. Altogether more than 40 Gt CO2 can be stored in (depleted) oil and gas fields in Western Europe and 150 to 1500 Gt CO2 of theoretical potential is estimated for deep saline aquifers in Western Europe [14]

CO_2 can be stored in three main types of underground formations: depleted reservoirs, deep saline aquifers and unconventional reservoirs (coal beds).

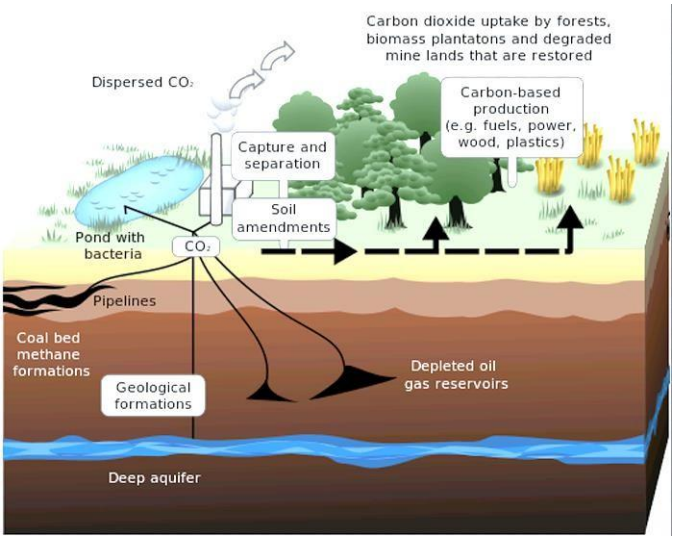

Figure 5 CCS storage types[15]

- Depleted gas and oil reservoirs

Oil and gas fields are made up of one or more reservoirs where brine has been replaced by hydrocarbons. When it is no longer possible to extract hydrocarbons, a reservoir is considered depleted. While the processes and seals that trap hydrocarbons in oil and gas reservoirs can also trap CO2, not every depleted reservoir will be suitable or available for CO2 storage. In addition to technical considerations, many jurisdictions restrict CO2 injection other than for the purpose of CO2-EOR in fields where some reservoirs are still being used for hydrocarbon extraction, in order to minimise the risk of negative interactions between the resource and CO2. In the near term, this could constrain the number of depleted oil and gas reservoirs available for dedicated CO2 storage. Reservoirs with ongoing oil and gas extraction are not suitable for dedicated CO2 storage, but they may be a target for CO2-EOR or hybrid approaches. Existing infrastructure (platforms, wells, pumping stations, etc.) could potentially be reused or to reduced decommissioning costs at the end of oil or gas extraction and reduced construction costs for the storage site. Existing infrastructure should be assessed to ensure that it is fit for purpose before a depleted reservoir is repurposed. As part of this, all legacy (i.e. pre-existing) wells will need to be assessed to ensure that they cannot become a pathway from which CO2 could leak. As of 2022, no dedicated CO2 storage is occurring in depleted fields. However, a number of projects are in development, including the Acorn project and the HyNet North West storage site, both off the United Kingdom, Project Greensand off Denmark, Porthos and Aramis, both off the Netherlands, the offshore Bayu-Undan project in Timor-Leste, the Ravenna hub off Italy, and the Moomba CCS project in the Australian outback.[16, 17]

- Saline aquifer formations

Saline formations, also known as saline aquifers, are porous and permeable sedimentary rocks that contain salty, non-potable water commonly known as brine. They are a common geological feature with wide geographic distribution. Some 98% of the world's estimated CO2 storage resources are in the form of saline aquifers and they offer significant theoretical storage capacity.

Saline aquifers are categorized into two main types: confined and unconfined (with open boundary conditions). Confined aquifers, similar to oil and gas reservoirs, trap fluids within specific geological formations such as structural features (e.g., anticlines) or stratigraphic elements (e.g., pinch-outs). These aquifers offer both vertical and lateral containment but generally have a lower storage capacity compared to unconfined aquifers, where fluids can move more freely in a lateral direction.[18]

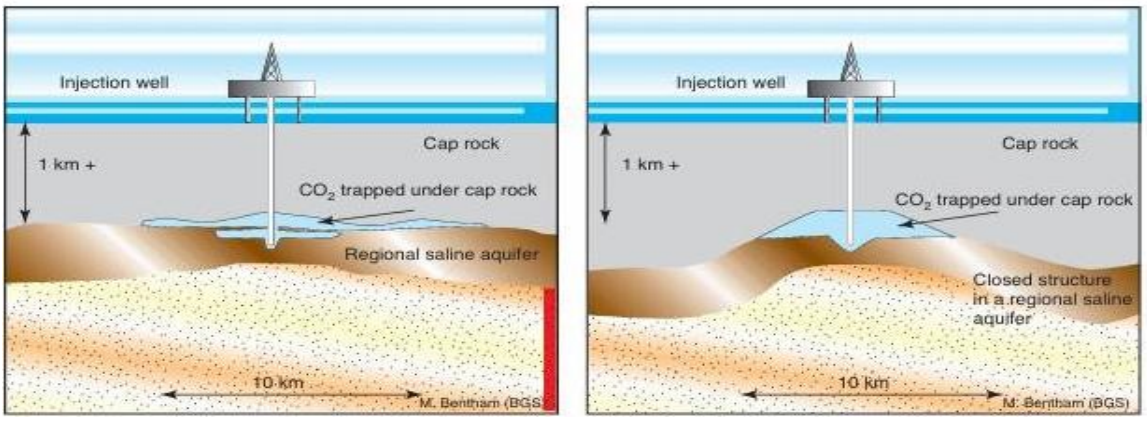

Figure 6 Unconfined and confined saline aquifers [19]

- Unconventional storage resources

Basalts and peridotites are igneous rocks and are reactive to CO2. When CO2 is injected, some of the rock dissolves and chemical reactions convert a proportion of the injected CO2 into solid minerals. Carbfix in Iceland operates the only active storage project in basalts and injected around 80 kt of CO2 between 2014 and the middle of 2022. The company aims to expand operations with the Coda Terminal, a project that will inject 300 kt CO2 per year starting in 2025. CO2 storage in basalts was also piloted in the United States during the Wallula Basalt Sequestration Pilot Project.

Unmineable coal seams can absorb CO2; however, methane is often released when CO2 is injected into them. Ongoing research is examining how effectively these deposits can store CO2.

Organic shales are a type of sedimentary rock rich in organic matter. Organic matter can absorb CO2 in a manner similar to coal. Limited work has been done to date on the technical and economic feasibility of using these resources for storage.[20]

Reservoir type	Lower estimate of storage capacity ($GtCO_2$)	Upper estimate of storage capacity ($GtCO_2$)
Oil and gas fields	675[a]	900[a]
Unminable coal seams (ECBM)	3-15	200
Deep saline formations	1000	Uncertain, but possibly 10^4

[a] These numbers would increase by 25% if "undiscovered" oil and gas fields were included in this assessment.

Table 1 Storage capacity for several geological storage options [21]

4. Trapping mechanisms

The capacity and injectivity of CO_2 storage are influenced by the geological and

petrophysical characteristics of the target formation. The underground trapping of injected CO_2 occurs through two primary mechanisms: physical trapping and geochemical trapping. The long-term effectiveness of CO_2 storage largely depends on the functionality and reliability of these mechanisms.

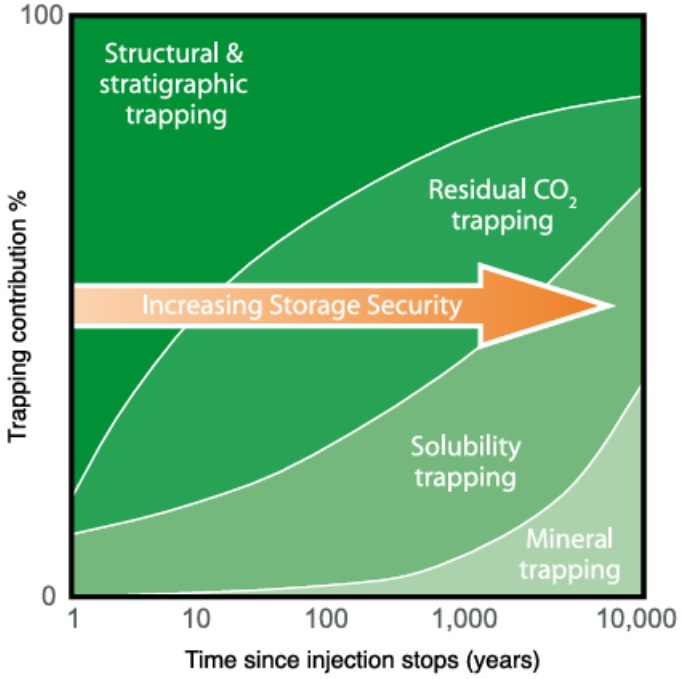

Figure 7 CO2 trapping mechanisms and storage security [22]

- Physical trapping mechanisms
    1) Structural/ Stratigraphic trapping

Initially,physical trapping occurs in low-permeability rocks (caprocks), such as shale or salt beds, is the primary means to store CO2 in geological formations that don't let them to escape. The underground spaces where this happens often have salty water, oil, or gas. Some traps are formed by bent or broken rocks (called structural traps), and some by changes in the type of rock (called stratigraphic traps). Both can hold CO_2 well, but it is important that not to inject too much pressure because it might break the seal or open the faults, letting the gas leak out..[23, 24]

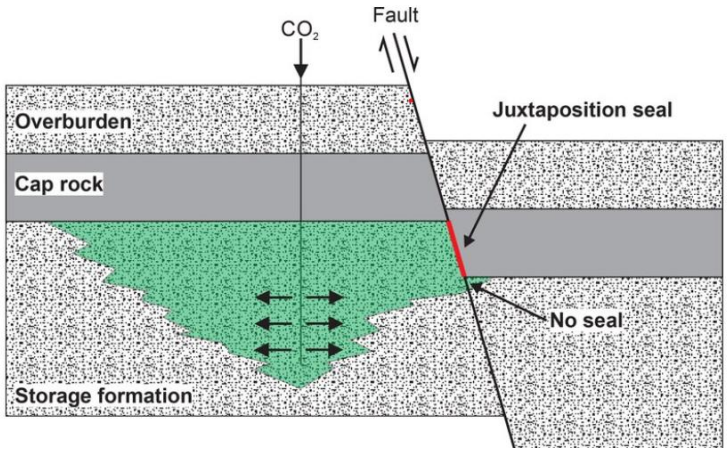

Figure 8 Impact of faults on plume migration in a CO2 storage site [1]

2) Residual trapping (hydrodynamic)

Hydrodynamic trapping usually occurs in formatayions that do not have anticline or fault and fluids can move very slowly through long distances.

in CO2 injection process,as CO2 has the lower density compared with water, it displaces saline formation water and then move upwards because of bouyancy forces. When it arrives the top of the formation, it migrate continuously as a separate phase until it is trapped in one of the structural or stratigraphic traps within the sealing formation. this saturation is called residual CO2 saturation..[24]

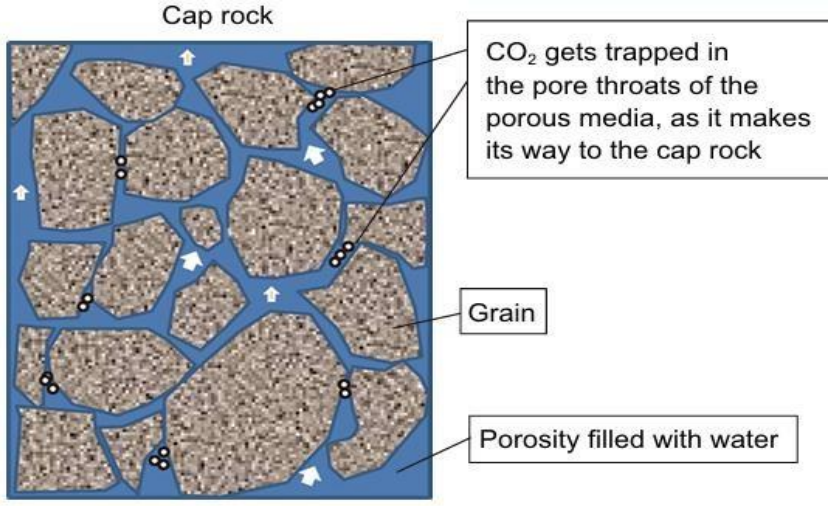

Figure 9 Residual trapping of CO2 [13]

- Geochemical trapping mechanisms

Carbon dioxide in the underground can experince a series of geochemical interactions with the both formation water and rock. this causes the increase of storage capacity and injection efficincy.

First, we have solubility trapping ,when CO2 dissolves in formation water. The important advantage of solubility trapping is that when CO2 is dissolved into water, it is no longer a separate phase, so the buoyant forces that drive it upwards removed totally. Next, as the rock starts to dissolve, CO_2 forms ions, and the pH level goes up. Finally, some fraction may be converted to stable carbonate minerals which called mineral trapping, the most permanent form of geological storage. .

Mineral trapping occurs slowly and can take a thousand of years or more. Nevertheless, the stability and efficiency of this trapping makes this a desirable option of long term storage. [24]

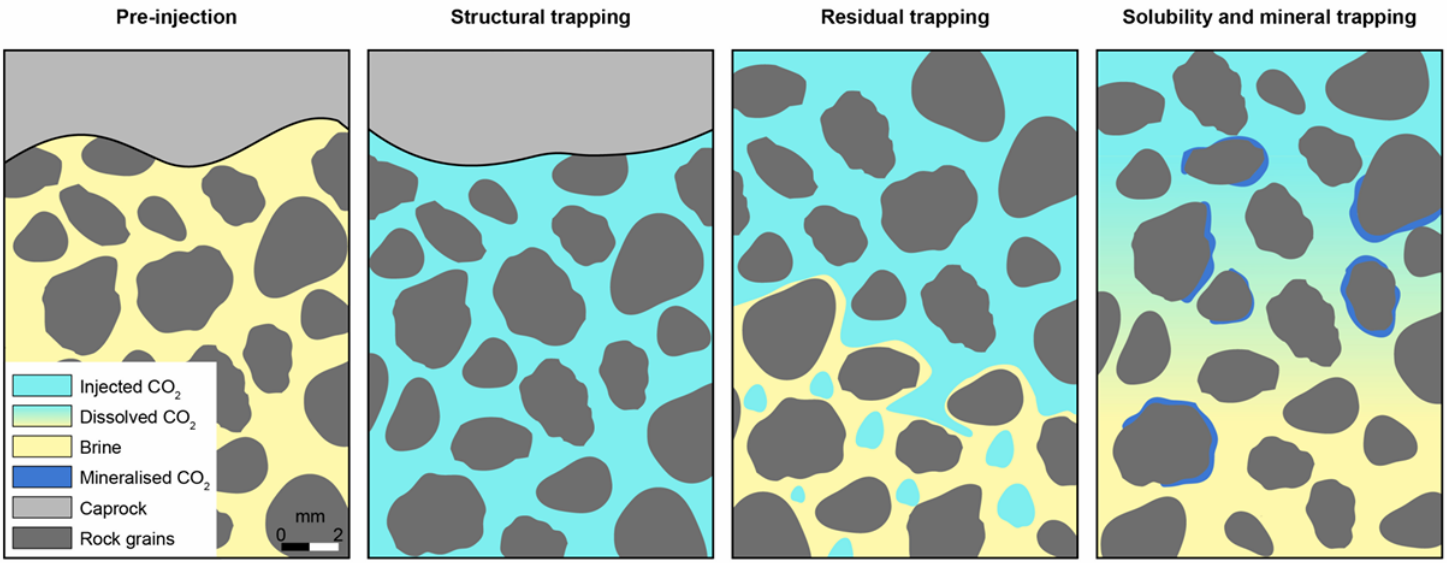

Figure 10 CO2 trapping within a reservoir on a microscopic scale[25]

5. Underground CO2 behavior

For underground CO_2 storage to work efficiently, it is important to understand the chemical behavior and thermodynamic environment of the reservoir

At normal temperature and pressure, carbon dioxide is a gas. but if temperature and pressure change it may be transform. At very low temperatures, CO_2 becomes a solid. If you warm it up until the pressure below 5.1 bar, it turns directly from solid to gas which is called sublimation.

Between −56.5 °C and 31.1 °C, if you compress CO_2 enough and remove the heat, it can become a liquid. The most important phase for engineers take place when the temperature goes above 31.1 °C and the pressure is higher than 73.9 bar, this is the supercritical state, where it behaves like both a gas and a liquid. In this state, it can be as dense as a liquid but still flow like a gas.

This special behavior of CO2 is very important in gas injection and storing CO_2 underground, because it lets us store more in a porous media.[26]

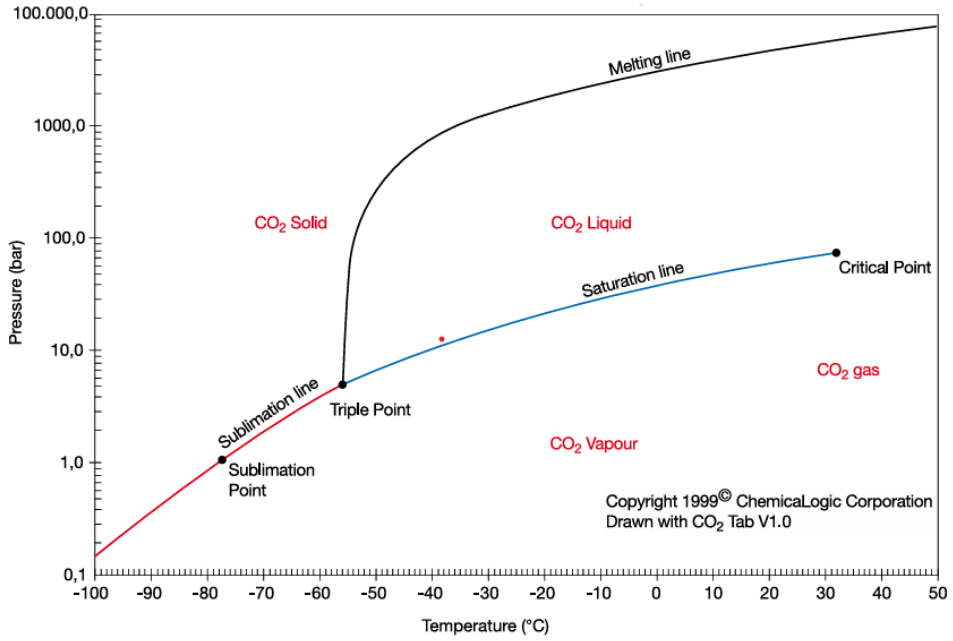

Figure 11 CO2 phase diagram.[27]

When carbon dioxide reaches a supercritical state, it behaves like both a gas and a liquid. It has a density close to that of a liquid but retains the low viscosity and flow characteristics of a gas. This combination gives supercritical CO_2 high mobility and high density, making it particularly well-suited for efficient underground storage.

The table below summarizes the supercritical state of CO_2 during injection and storage.

CO_2 Supercritical State Conditions	**Values**
Temperature	31 °C
Pressure	73.9 bar
Density	850 Kg/m^3
Depth	Below 800 m

Table 2 CO2 supercritical phase conditions

The phase behavior and physical characteristics of CO_2, such as its density and viscosity, are highly influenced by variations in pressure and temperature, as illustrated in the accompanying graphs. Notably, the relationship between density, viscosity, and these variables plays a critical role in determining the feasibility of underground CO_2 storage and its injectivity, which will be explored further in this study.

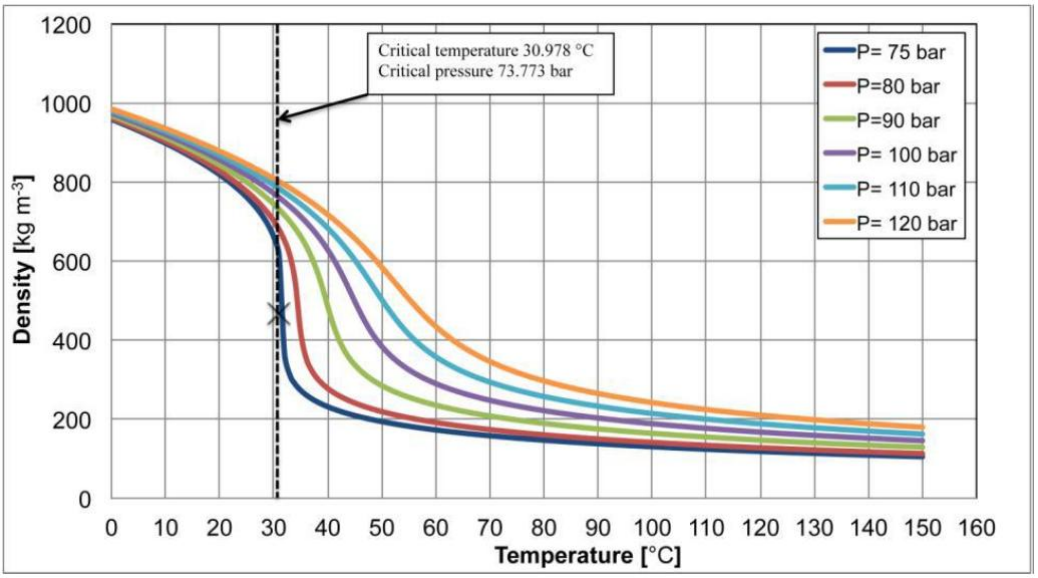

Figure 12 Supercritical carbon dioxide density as a function of the pressure and temperature [28]

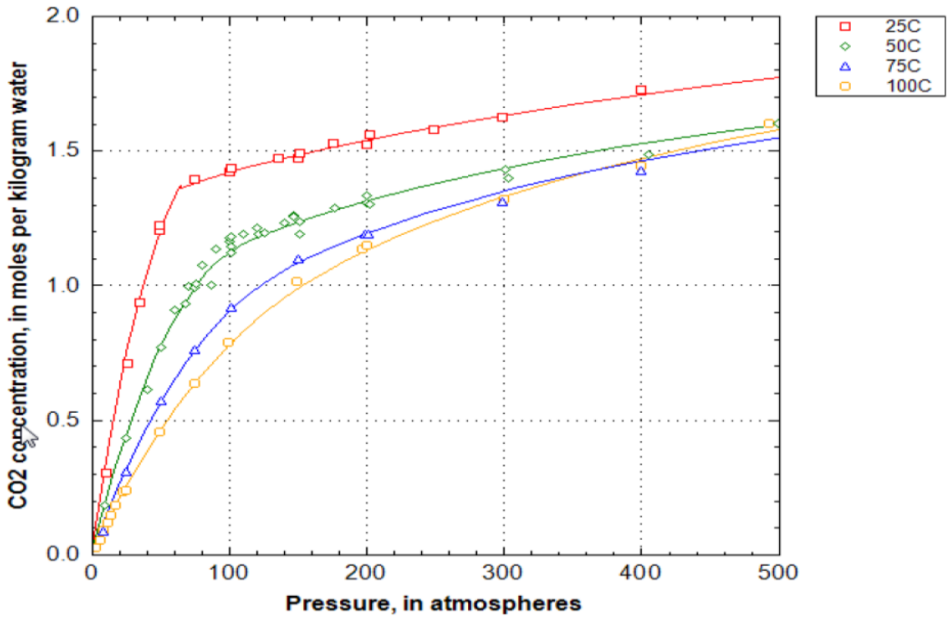

Figure 13 CO2 concentration in different pressures and temperatures [29]

CO_2 solubility is strongly influenced by the specific pressure and temperature conditions . As illustrated in the graph, CO_2 solubility increases with rising pressure but decreases as temperature increases [30]. Additionally, higher water salinity reduces CO_2 solubility due to the "salting-out" effect, where dissolved salts limit the amount of CO_2 that can dissolve in water. This relationship between water salinity and CO_2 solubility is crucial for the solubility trapping potential of CO_2 in water-bearing reservoirs, such as those containing mobile or connate water.

6. Numerical simulation and modeling

For simulation CO2 storage in underground reservoirs, we use numerical modelling which propose 3D static geological model of the rock mass. there are many different softwares to simulate the CO2 injection which oil and gas industries use. the results of numerical simulations determine the CO2 storage capacity and knowing that this site is suitabe for storge or not in terms of economic and safty so they are a key element in the decision-making process when considering the implementation of CCS projects on an industrial scale.[33]

Thus, Numerical simulation software tools play a crucial role in this context, providing advanced features to simulate multiphase fluid dynamics, geochemical interactions, and geomechanical behaviors in complex, varied subsurface settings. For instance, tools like tNavigator, OPM, and ECLIPSE are designed to simulate how CO_2 behaves under various reservoir conditions and injection methods..

In this research, we simulate CO2 injection using two different softwares, first we use Open Porous Media (OPM) and in the following compare the result with tNavigator. OPM is an open-source simulator which designed for reservoir simulation, particularly for carbon capture and storage (CCS). OPM was initially founded as a collaboration between groups at Equinor , SINTEF, the University of Stuttgart, and the University of Bergen, but over time, several other groups and individuals have joined and make it stronger. What today forms the OPM suite of software, has mainly been developed by SINTEF, NORCE (formerly IRIS), Equinor, Ceetron Solutions, Poware Software Solutions, and Dr. Blatt HPC-Simulation-Software & Services.[34] tNavigator is a commercial, integrated reservoir simulation platform developed by Rock Flow Dynamics (RFD), a company founded in 2005 that provides advanced tools for CCS simulation with high computational efficiency. The results obtained from these simulations will be analyzed and compared to evaluate their performance and accuracy.

7. Objectives of the thesis

This thesis use two different sofwares to simulate the CO2 injection process in underground reservoir with saline aquifer. At the start, we create a base model which will explain later in OPM. main reservoir properties such as depth, convective dissolution, critical gas saturation, and relative permeability were changed one by one to see how they affect CO_2 injection and storage. The result of our simulation are total gas in place, reservoir pressure, and other relevant parameters.

In the second phase of the study, we create the same model in tNavigator. The aim was to compare the results of tNavigator with those obtained from OPM. We do this to know which software show the better performance and the difference of result in two software in the same model.and how accurate they are for carbon capture and storage (CCS) simulations.

II. Models' description

The model created in this thesis is a saline aquifer reservoir.At the first, the reservoir is fully saturated with water.

The 3D view of our model is shown in figure 15. The model includes 20 blocks in x-axis, 21 blocks in y-axis, and 20 blocks in z-axis, so we have total of 8400 grid blocks (20*21*20). Each grid cell has 20 meters in the x-direction, 20 meters in the y-direction, and 5 meters in the z-direction. The reservoir's top is positioned at a depth of 2000 meters.

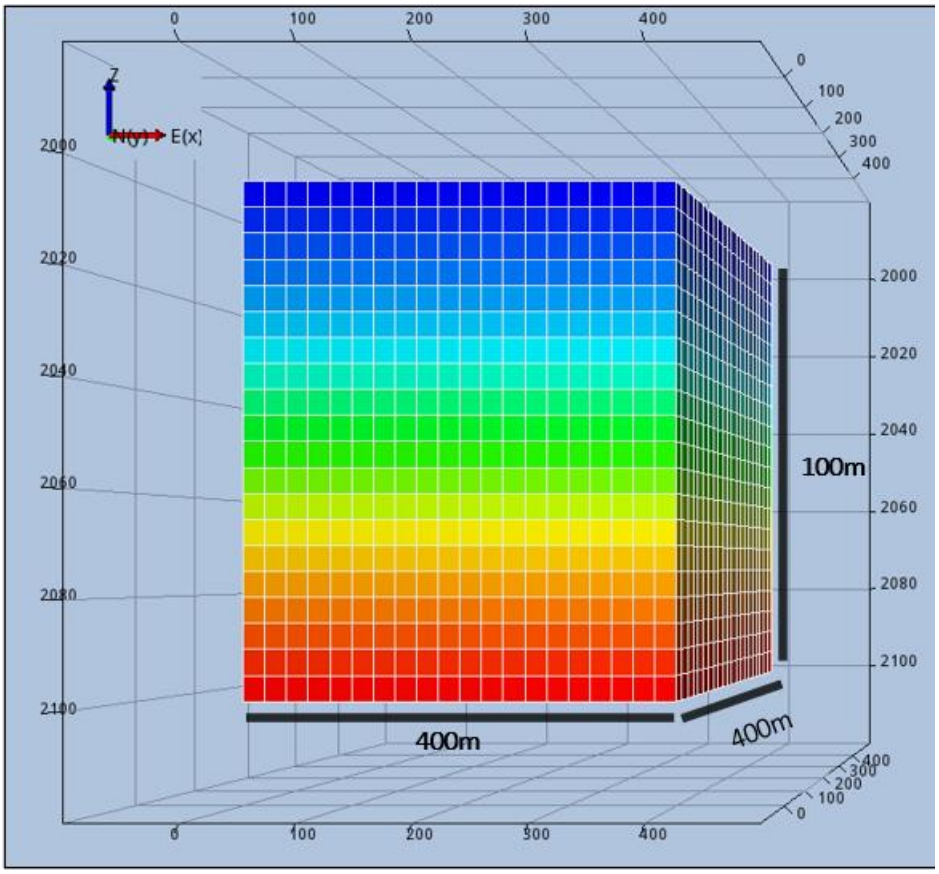

Figure 14 3D representation of reservoir model.

1. Rock fluid parameters

Table 3 provides a summary of the rock and fluid properties, including porosity and permeability. As indicated in the table, the reservoir exhibits homogeneous and isotropic characteristics.:

Parameter	**Value**
Porosity	30%
Kx	2000 mD
Ky	2000 mD
Kz	2000 mD
TOP	2000 m
Salinity	35 g/l
Rock compressibility	1e-6 1/bar
Initial pressure (Pi)	200 bar
Gas-Water contact(GWC)	2500 m
Temperature	50 ˚C at the depth 100m
Gas specific gravity	0.5562

Table 3 Average parameters value

2. Simulation with Open Porous Media software (OPM)

The Open Porous Media (OPM) is a project that coordinates cooperative development, maintenance and distribution of an open-source software focused on CO2 storage and improved and enhanced oil recovery along with maintenance and distribution of open data sets. Flow can be coupled with MOOSE (the geochemistry module). The software support standard industry formats for input and output files (ex. Eclipse) and provides a visualization tool called ResInsight. Moreover, the results can be exported in Vtk format for visualization in ParaView.

The extended black-oil model included in Flow has two main advantages, with respect to a fully compositional model:

- Reduced computational time
- Possibility to include CO2 injection in existing reservoir simulation models

The standard black oil model considers three pseudo components: oil, gas and water. Gas can dissolve into the oil phase and oil vaporize into the gas phase depending on the pressure, but oil and gas cannot enter the water phase. –

The main black-oil model equations are:

- mass conservation equation for phase α:

$$\partial/\partial t(\phi A_\alpha) + \nabla \cdot u_\alpha = Q_\alpha$$

$A_w = b_w \cdot S_w$	$u_w = b_w \cdot v_w$	Water	
$A_o = b_o \cdot S_o + r_v \cdot b_g \cdot S_g$	$u_o = b_o \cdot v_o + r_v \cdot b_g \cdot v_g$	Oil	
$A_g = b_w \cdot S_w + r_s \cdot S_o$	$u_g = b_g \cdot v_g + r_s \cdot v_o$	Gas	[35, 36]
$A_s = b_s \cdot S_s$	$u_s = b_s \cdot v_s$	Solvent	

- Darcy law:

$$v_\alpha = -(k_{r\alpha e} / \mu_{\alpha e}) \cdot K \cdot (\nabla p_\alpha - \bar{\rho_\alpha} \cdot b_\alpha \cdot g)$$

The effective relative permeabilities $k_{r\alpha e}$ and viscosities $\mu_{\alpha e}$ incorporates the degree of miscibility of the fluids and the sub-grid scale fingering effects by interpolating between properties for the fully miscible and the immiscible case.

The interpolation function *M* both depends on the fluid saturations and the pressure

$$k_{roe} = M \cdot ((S_o - S_{or})/(S_n - S_{gc} - S_{or})) \cdot k_{rm} + (1 - M) \cdot k_{ro}$$

While the effective gas and solvent relative permeabilities defined as:

$$k_{rge} = M \cdot ((S_g + S_s - S_{gc})/(S_g + S_s)) \cdot k_{rm} + (1 - M) \cdot k_{rg}$$

$$k_{rse} = M \cdot ((S_g + S_s - S_{gc})/(S_g + S_s)) \cdot k_{rm} + (1 - M) \cdot (S_s / (S_g + S_s)) \cdot k_{rs}$$

Effective viscosities are defined as below where ω, the Todd-Longstaff mixing parameter, is used to interpolate between a fully stable displacement (ω=0) and a non-stable displacement with fingering effects (ω=1). The fully mixed viscosities for oil and solvent (μ_{mos}) gas and solvent (μ) and oil, gas and solvent (μ_m) are computed based on the standard mixing rules

$$\mu_{oe} = \mu_o^{(1 - \omega)} \cdot \mu_{mos}^{\omega}$$

$$\mu_{ge} = \mu_g^{(1 - \omega)} \cdot \mu_{msg}^{\omega} \qquad [35, 36]$$

$$\mu_{se} = \mu_s^{(1 - \omega)} \cdot \mu_m^{\omega}$$

If CO2 is injected in a depleted hydrocarbon reservoir, to distinguish the formation gas from the injected CO2, a forth component representing the injected CO2 is added to the black-oil model. The degree of mixing of the injected CO2 with reservoir oil is given as an input parameter that depends on the fraction of the CO2 and the pressure in the reservoir.

In addition, for CO2 storage scenario, carbon dioxide and water phase solubility is accounted for. To this end, a dedicated keyword CO2STORE is adopted. Under this option, analytical CO2-Brine PVT internal model from literature is adopted, rather than interpolation from tabulated values [36]. A full description of the underlying PVT models is described by Sandve et al [37]. As a consequence, the normal PVT keywords like DENSITY, PVTO, PVDG etc. are not required and if entered will be ignored by the simulator. Note that the CO2-Brine PVT properties depend on the temperature and salinity and these must therefore be entered in the PROPS section. The reservoir temperature can be defined using, e.g., the RTEMP keyword. Region based salinity can be provided using the SALINITY keyword.

For CO2 storage in aquifer, the CO2STORE keyword must be used together with either: (1) the GAS and WATER keywords (or alternatively the GASWAT keyword), or (2) the GAS and OIL keywords in the RUNSPEC section. The DISGASW keyword in the RUNSPEC section can be used with option (1) to model dissolution of CO2 in the Brine. Option (1) has the advantage that it can be used with the VAPWAT and PRECSALT keywords in the RUNSPEC section to model the impact of both vaporization of residual water and salt precipitation in the near wellbore region on injectivity of CO2 injection wells.

In option (1), the GAS and WATER (or GASWAT) keywords declare that the gas and water phases are present in the model. When the CO2STORE option is used, the water phase represents the brine and the gas phase represents CO2. Note that the input and output keywords need to be consistent with this assumption, e.g., GSF (gas saturation function) and WSF (water saturation function) should be used for the CO2-Brine relative permeability, etc.

In option (2), the GAS and OIL keywords declare that the gas and oil phases are present in the model. Internally when CO2STORE is used, the oil phase refers to the brine and the gas phase to CO2. Again, the input and output keywords need to be consistent with this assumption, e.g., SGOF (gas-oil relative permeability) is used for the CO2-Brine relative permeability, FOIP (Field Oil-In-Place) shows the total amount of brine in the reservoir, etc. Option (2) currently has the advantage that it can be used with the DRSDTCON keyword in the SCHEDULE section to control convective dissolution of CO2 into the in-situ brine. Support for the use of DRSDTCON with option (1) is planned to be added in the next release.[36]

In this study, option (2) was selected within the OPM simulator, using the GAS and OIL keywords to represent the CO_2 and brine phases, respectively. This model enables the use of the DRSDTCON keyword in the SCHEDULE section to model the convective dissolution of CO_2 into the brine. Under the CO2STORE keyword, the simulator internally assigns the oil phase to brine and the gas phase to CO_2, allowing for suitable managing of the two-phase system.

On the other hand, in tNavigator, the CO_2 storage option is used. In this model, the simulator uses the water phase as brine and the gas phase as CO_2, without requiring the oil phase explanation

III. Simulation Result

The model described in section II is considered as the base model. It defines a datum depth of 2000 meters with a pressure of 200 bar and the WATCONT value is set to 2500 meters. As previously mentioned, oil represents brine for OPM in the black oil model with keyword CO2STORE option. As a result, the entire modeled reservoir is initially filled with brine only, and no free CO_2 is present at the beginning of the simulation. The temperature of the reservoir is considered as 50 °C. The injection well is located in layer 20 at coordinates (1, 11, 20). In this case, no skin effect is considered. Gas is injected from the surface at a rate of 1000 Sm^3/day, with a maximum bottom-hole pressure constraint of 250 bar. The project started on January 1, 2019, and the simulation is conducted for a duration of 20 years. The other parameters in the model were said in the previous section. The location of the injection well is shown in figure 16.

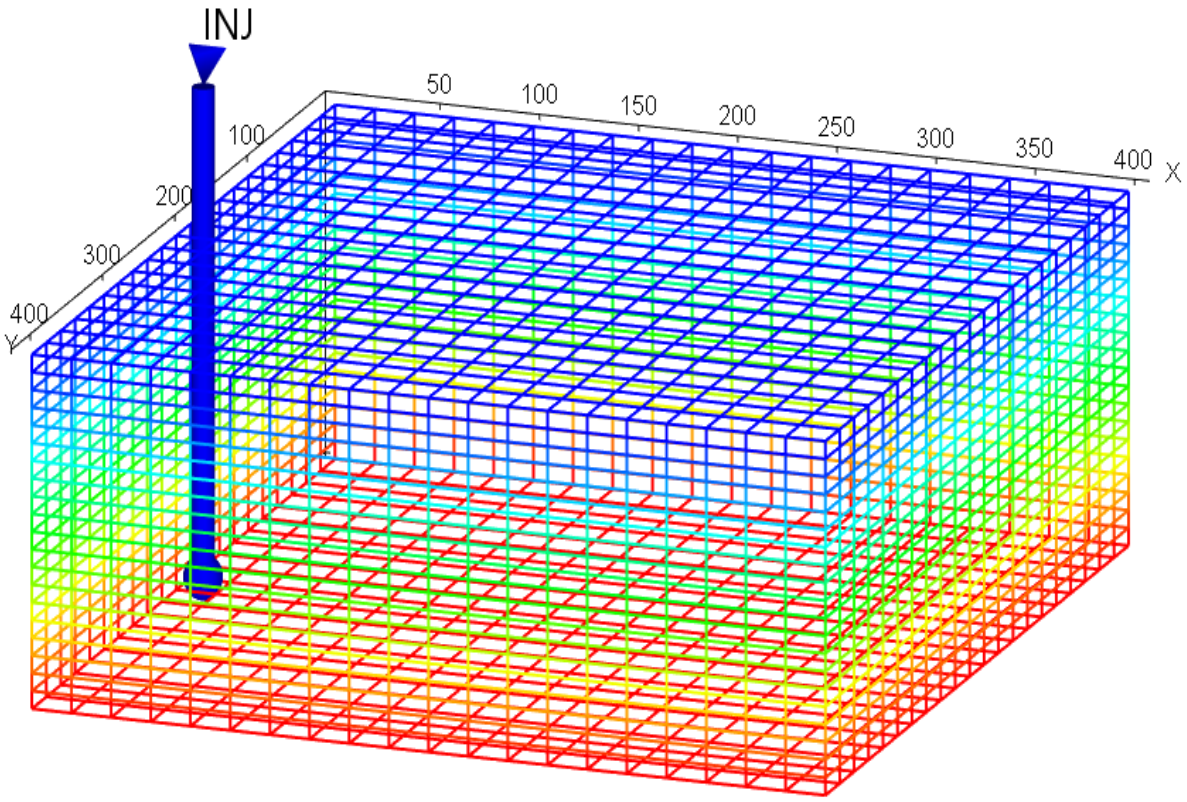

Figure 15 The location of the injection well.

We consider three grid blocks along the injection well—top (1, 11, 1), middle (1, 11, 10), and bottom (1,11, 20)—and calculate properties such as pressure, gas saturation, and gas in place during the gas injection process.

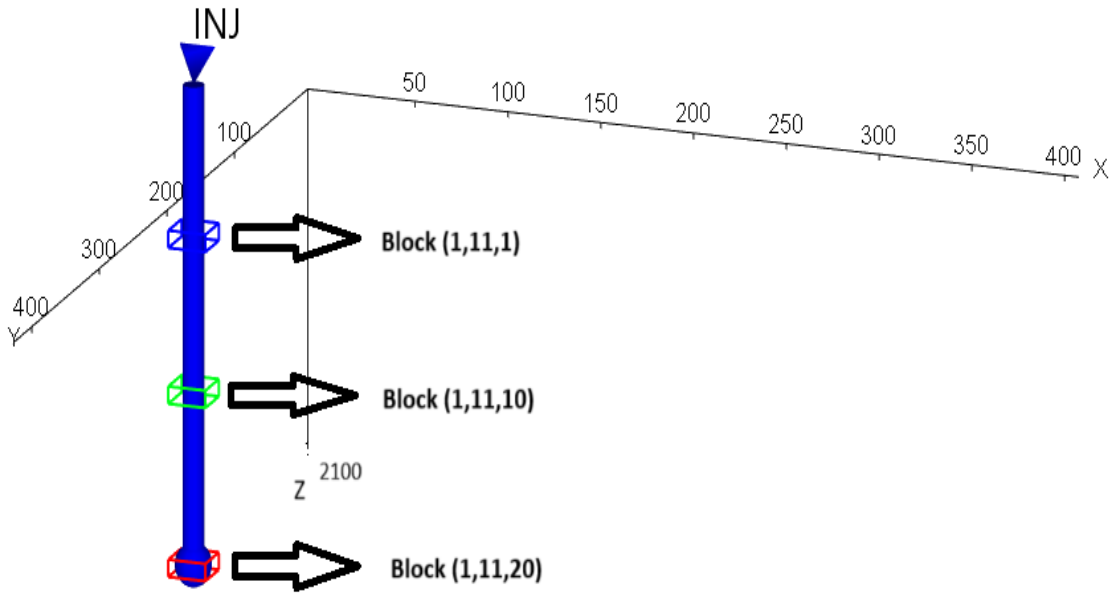

Figure 16 The location of monitoring grid blocks

1. Convective Dissolution

The dissolution of CO2 into brine is an important effect that must be considered. The main mechanism that drives the dissolution is convective mixing. Phase segregation causes the lighter CO2 moves quickly to the top of the reservoir and then migrates along the sealing layer. For field scale simulations a typical grid block size is tens or even hundreds of meters in the horizontal direction and typically a few meters in the vertical direction. The density difference between CO2 in gas (or super critical) phase and brine leads to rapid phase segregation. The lighter CO2 moves quickly to the top of the reservoir or to an intermediate sealing layer and then migrates along the sealing layer. For cells where a vertical equilibrium is reached only the top layer of the cell is exposed to the free CO2 and a fully mixture of the CO2 and brine cannot be assumed. A direct use of the solubility models will thus over-estimate the amount of dissolved CO2 in brine in these cells if used directly. The dissolution process in these cells is controlled by the convective mixing. Since brine with dissolved CO2 is slightly heavier than without, instabilities will occur at the phase boundary in form of heavier fingers of brine with dissolved CO2 migrating downwards. These fingers happen on the centimeter scale and can therefore not be included directly in field-scale simulations. Instead, the effect of convective mixing is included through a control of the dissolution rate. The convective mixing depends on both dynamic and static properties of the reservoir but dimensional analyses suggested a scaling for the dissolution rate that allows for usage of a single parameter.[37]

DRSDTCON keyword on OPM software is a real positive number that defines a dimensionless parameter (X) that controls convective dissolution of carbon dioxid into brine. A value of zero means that convective dissolution of CO2 into in situ brine does not occur and free CO2 cannot dissolve into the brine in a grid cell. Alternatively a non-zero value of DRSDTCON allows convective dissolution of CO2. To examine the impact of upscaled convective mixing, a dimensionless dissolution coefficient of $\chi = 0.034$ was applied and compared to a reference case in which CO_2 dissolution is neglected. The results indicate that, during the injection period, approximately 0.5% of the injected CO_2 dissolves into the brine each year. This dissolution rate corresponds to roughly one-third of the upper bound estimate of 1.8% per year, as derived from gravity monitoring data.[37]

Figure 18 presents a comparison of the total field gas injection volume (in m^3) over time for four different scenarios. The "Normal" case refers to the scenario without convective dissolution keyword, it means fully dissolution. The other three cases incorporate convective dissolution with different dimensionless parameter (DRST) of 0.04, 0.4 and 1 respectively, while applying a well bottom hole pressure (WBHP) constraint of 300 bar. The results indicate that convective dissolution has a minimal impact on the total field gas injection volume under the given conditions.

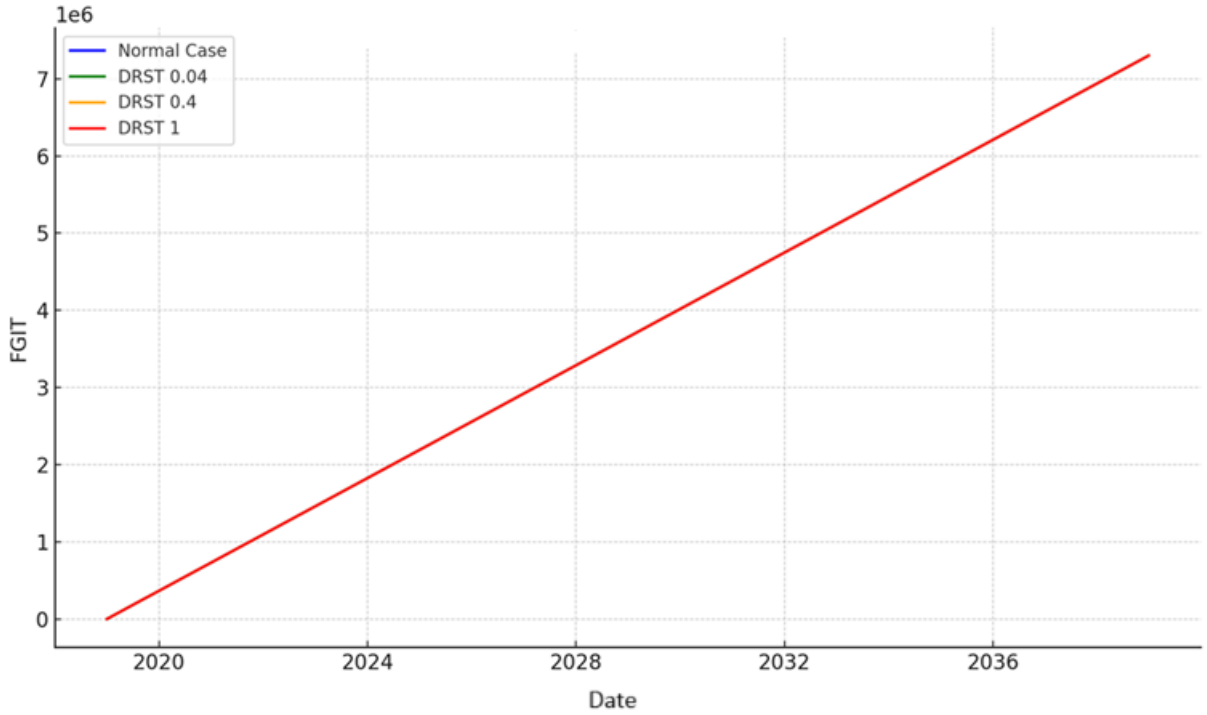

Figure 17 Field Gas Injection total(FGIT m3) vs date for different DRST values with WBHP=300bar

Figure 19 illustrates the field average pressure (in bar) over time for this scenario. The results indicate that reduced convective dissolution leads to an increase in the average reservoir pressure. This is because the gas dissolves slowly into the water, and as a result, more undissolved gas accumulates in the reservoir, leading to an increase in pressure.

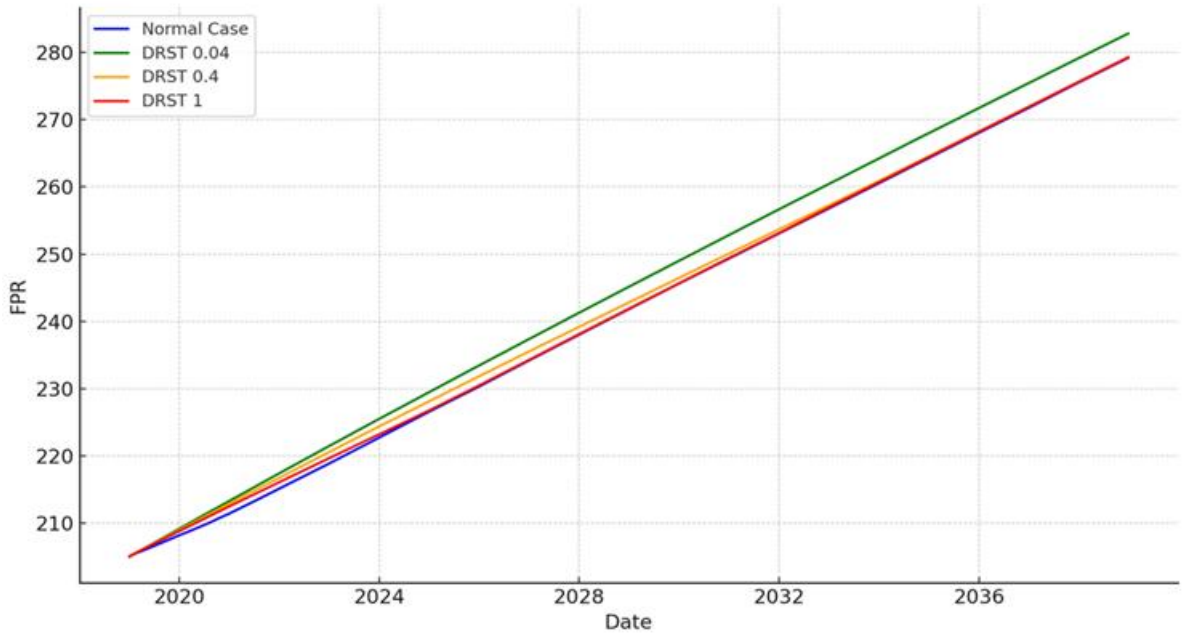

Figure 18 Field Average Pressure vs date for different DRST values with WBHP=300bar

The well bottom hole pressure (WBHP) constraint is now reduced to 250 bar, and the results are compared with the previous case in which the WBHP was set to 300 bar. In this case, lower

convective dissolution leads to a reduction in the total field gas injection and an increase in the average reservoir pressure. This is due to the WBHP constraint of 250 bar, which limits the allowable pressure at the injection well. As convective dissolution is reduced, less gas dissolves into the formation water, resulting in greater resistance to injection. Consequently, the amount of gas that can be injected decreases, while the undissolved gas accumulates and causes the reservoir pressure to rise.

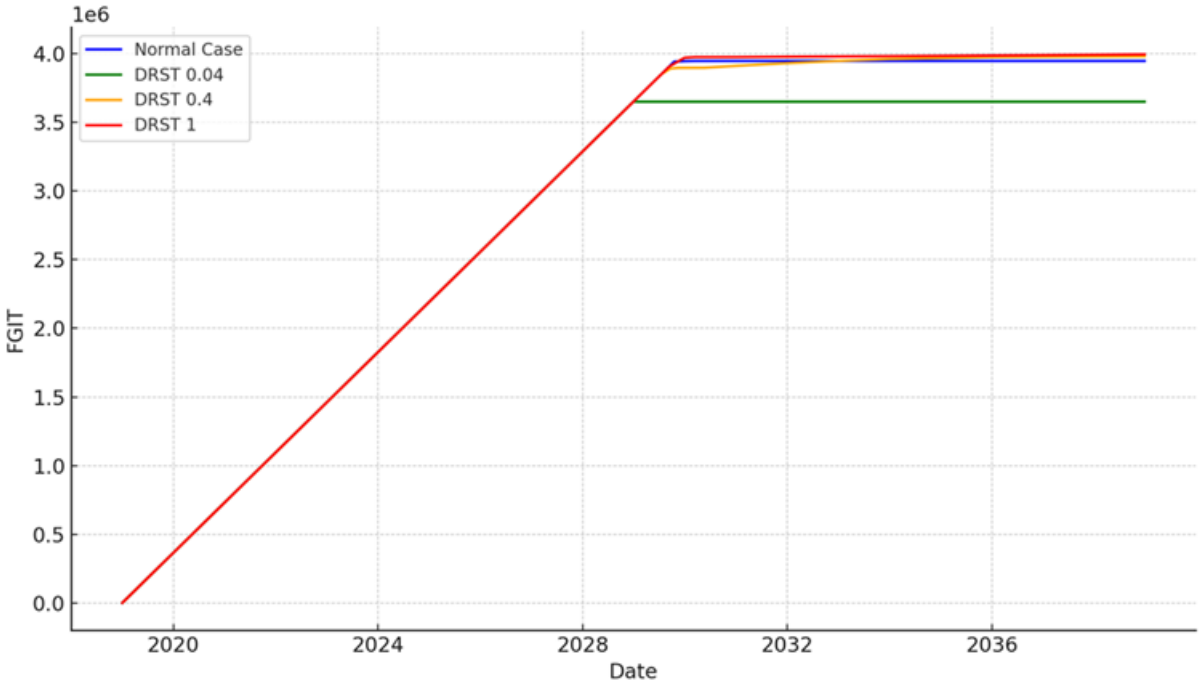

Figure 19 Field Gas Injection total(FGIT m3) vs date for different DRST values with WBHP=250bar

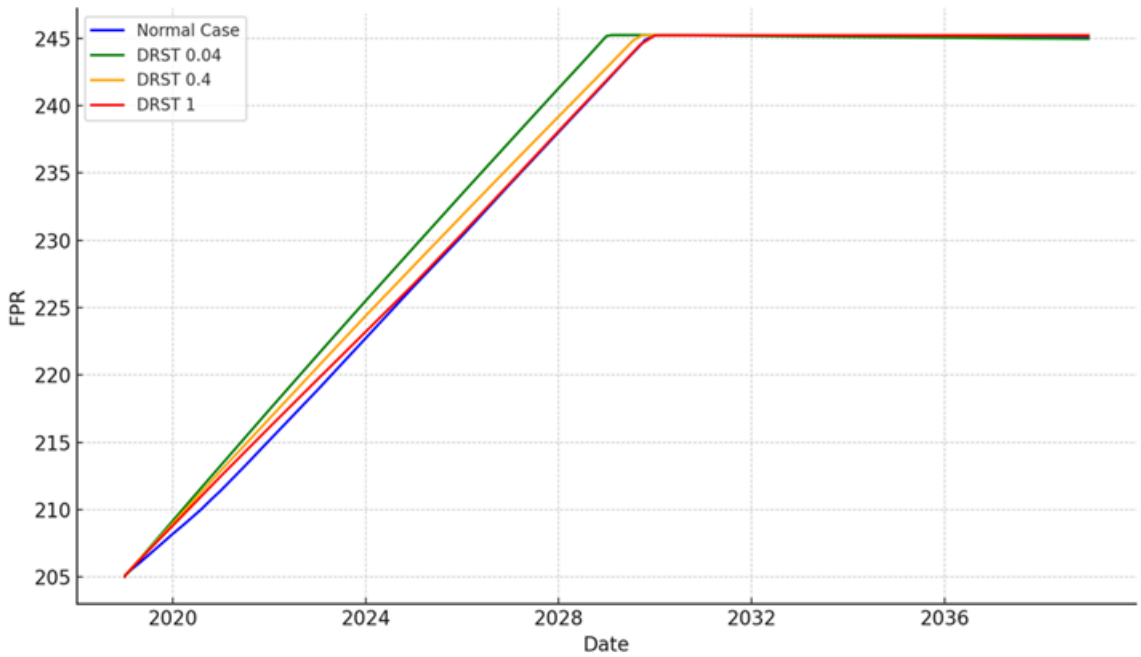

Figure 20 Field Average Pressure vs date for different DRST values with WBHP=250bar

2. Sensitivity analysis

In this section to see the effect of different parameters on injection process, sensitivity analysis will be performed.

Critical gas saturation (Sgc) is a important parameter in reservoir engineering, espicially during gas injection processes such as enhanced oil recovery (EOR) and carbon capture and storage (CCS). It defines that minimum gas saturation that require for CO2 to start flowing. Below the Sgc the gas cannot move and remain in the reservoir and when the saturation of the gas reaches this value, gas start flowing.

For CCS projects, understanding Sgc helps in risk analysis of CO_2 movement and potential leakage. Monitoring gas saturation levels relative to Sgc is important in choosing injection strategies and optimize efficincy .

In this study, we analyse the impact of different Sgc into reservoir simulations by changing parameters in the base model, as summarized in Table 4. Two scenarios are considered: one without considering for Sgc and another with Sgc set to 0.15. The objective is to monitor changes in block gas saturation, injection rate and pressure under these differing conditions. This analysis of critical gas saturation show the role of Sgc in forcasting gas mobility and enhancing injection efficiency.

Parameter	**Value**
Porosity	30%
Kx	500 md
Ky	500 md
Kz	50 md
TOP	2000 m
Gas injection rate	10000 Sm^3/day
WBHP constraint	240 bar
Initial pressure (Pi)	200 bar
Gas-Water contact(GWC)	2500 m
Injection Duration	31 months
Shut-in the well	31 months

Table 4 Average parameters value

2.1. Block Gas Saturation:

The results are presented in Figures 22, 23, and 24. Since the injection well is located in the lower block, the injected gas tends to migrate upward due to gravitational forces. As a result, gas saturation in the upper block is higher compared to the lower blocks. Another important observation is related to the imposed critical gas saturation (Sgc) of 0.15. In this case, gas begins to move only after reaching the critical saturation, leading to a delay in its migration. Consequently, when gas injection is stopped, the gas saturation in the lower block is higher than in the scenario where no critical gas saturation is considered.

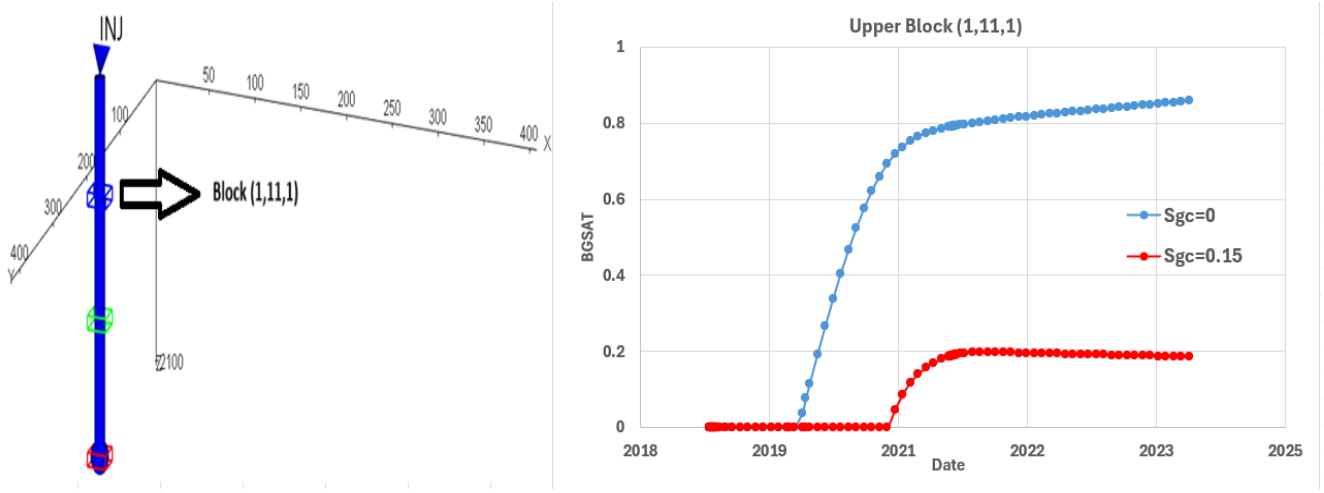

Figure 21 Block gas saturation vs Time for upper block (1,11,1)

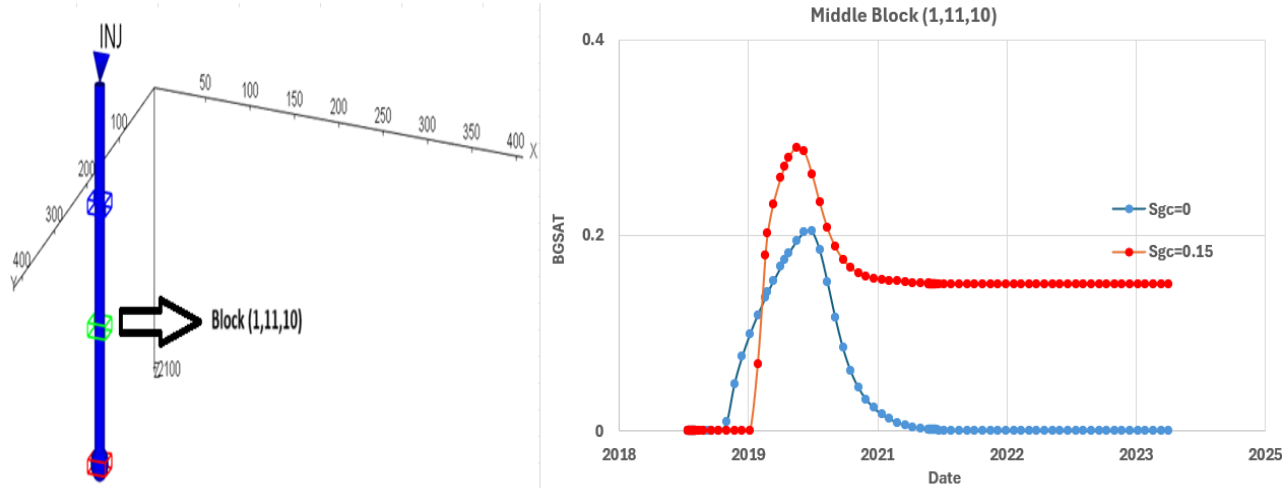

Figure 22 Block gas saturation vs Time for middle block (1,11,10)

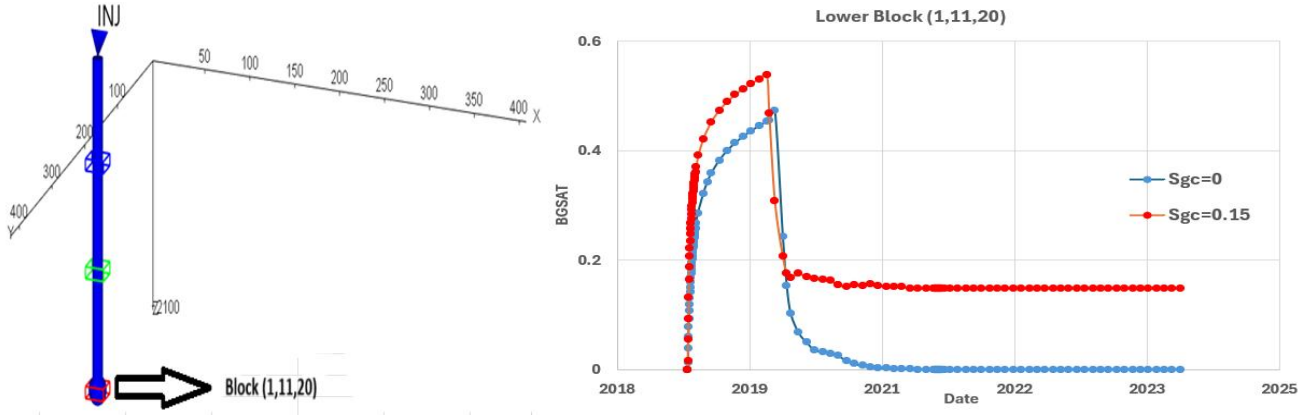

Figure 23 Block gas saturation vs Time for lower block (1,11,20)

2.2. Well Bottomhole Pressure (WBHP) and Well Bottom Pressure (WBP):

In figure 25 The left plot presents the Well Bottom Hole Pressure (WBHP), while the right plot

displays the One-point Pressure Average, representative of the Well Bottom Pressure (WBP). During the injection phase (2019 to mid-2021), the WBHP exhibits a steady increase from approximately 210 to 240 bara (which is set as pressure constraint), reflecting the dynamic pressure buildup at the bottom of the well due to continuous gas injection. In contrast, the WBP shows a smoother, gradual increase over the same period, capturing the average reservoir pressure increase near the wellbore.

Following the stop of injection (mid-2021 onward), the WBHP drops sharply to zero. This apparent drop does not imply a physical pressure depletion but rather indicates the absence of flowing conditions—WBHP is undefined or unmeasurable in the absence of injection or production. Meanwhile, the WBP remains nearly constant at ~240 bar throughout the shut-in period. This plateau signifies that, with no further injection or extraction, the reservoir pressure has reached a new equilibrium and stabilizes at its post-injection level.

Overall, the differing behaviors of WBHP and WBP highlight the distinction between dynamic (flowing) and static (average) pressure measurements, emphasizing the importance of context when interpreting well pressure data in simulation studies.

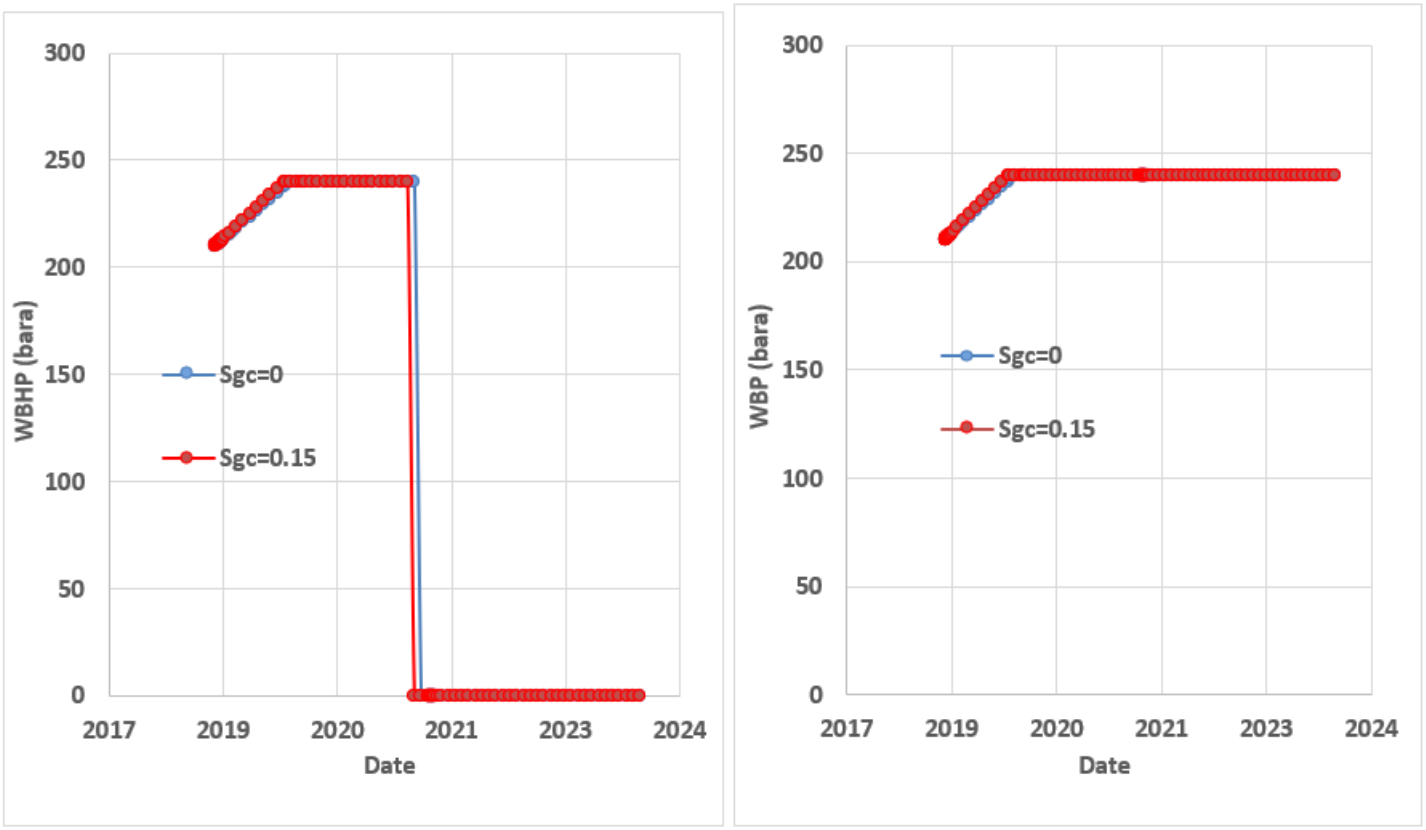

Figure 24 well bottom hole pressure (WBHP-left plot) and well bottom pressure (WBP-right plot) vs Date.

As shown in the figure, the critical gas saturation does not affect the normal trends of WBHP or WBP. This is expected, because critical gas saturation firstly affect gas mobility and relative permeability, instead of pressure propagation in the absence of phase change or flow. Since gas injection increases pressure but does not yet cause gas to move as a mobile phase below the critical saturation, the effect on both WBHP and WBP remains negligible in this simulation.

2.3. Total Gas Injection (WGIT) and Gas Injection Rate (WGIR):

Figures 26 and 27 display the total gas injection (WGIT) in Sm^3 and the daily gas injection rate (WGIR) in Sm^3/day respectively during the same simulation period using two different critical gas saturation scenarios: Sgc = 0 and Sgc = 0.15

In Figure 26, both scenarios show a fast increase in total gas injection starting from 2019, reaching a plateau after the injection period ends. The scenario with Sgc = 0 attains a higher total gas injection (~3.6 million Sm^3) compared to Sgc = 0.15 (~3.0 million Sm^3). This difference is caused by the effect of relative permeability due to non-zero critical gas saturation, because as gas saturation increases and the critical threshold is crossed, part of the gas becomes immobile and gas mobility and overall injectability decrease.

Figure 27, displays the injection rate, shows this effect better. During the early injection period, both scenarios inject at a nearly constant maximum rate (~10,000 Sm^3/day), which corresponds to operational or facility constraints. However, as the reservoir pressure builds up and mobility becomes restricted (especially in the Sgc = 0.15 case), both rates decline. Notably, the decline in injection rate occurs more rapidly and steeply in the Sgc = 0.15 scenario, confirming that gas becomes harder to inject as immobile saturation increases resistance to flow.

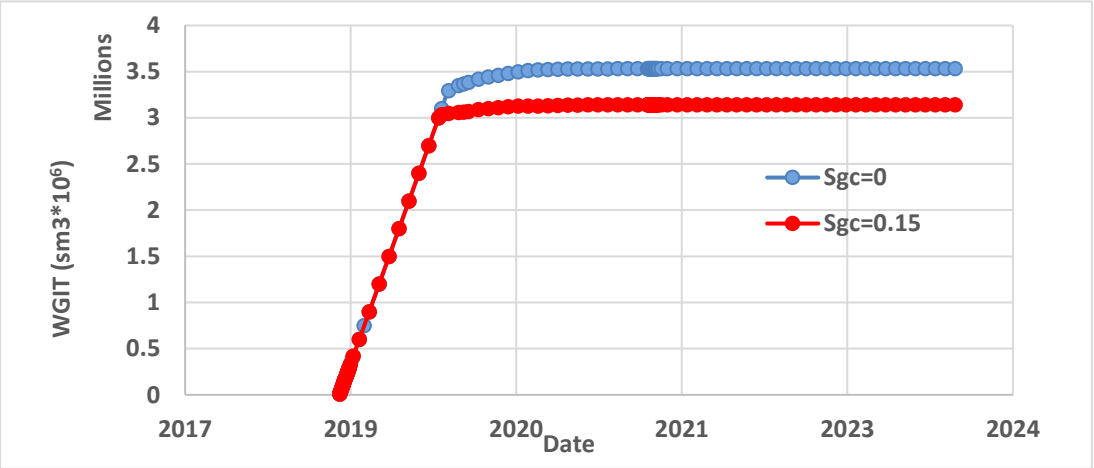

Figure 25 Total gas injection (WGIT) in Sm^3 vs Date for Sgc=0 and Sgc=.015

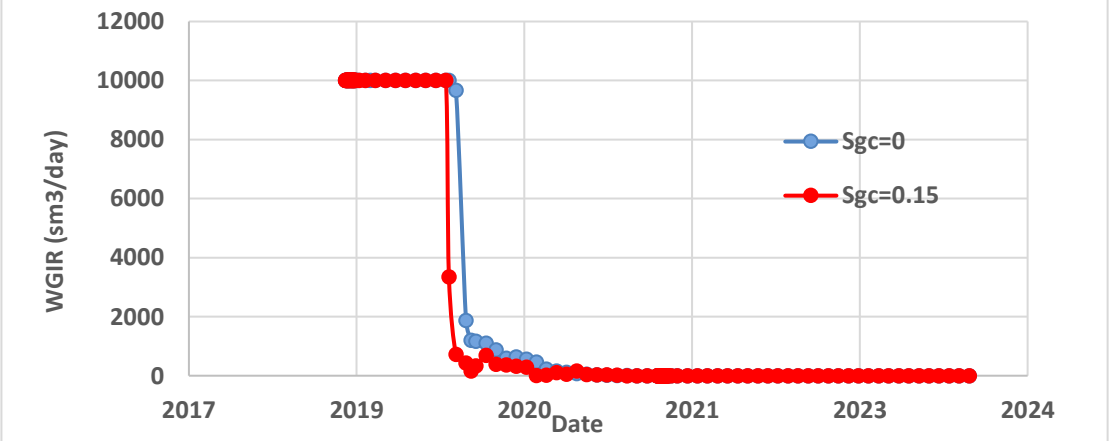

Figure 26 Gas injection rate (WGIR) in Sm^3/day vs Date for Sgc=0 and Sgc=.015

Together, these plots demonstrate that a non-zero critical gas saturation significantly reduces both the sustained injection rate and the ultimate gas storage capacity. These results emphasize the importance of incorporating accurate critical saturation values into simulation models to reliably predict reservoir performance during CO_2 injection operations.

2.4. Field Gas In Place (FGIP):

Figure 28 shows the Field Gas In Place (FGIP) for two different critical gas saturation values: Sgc = 0 (blue curve) and Sgc = 0.15 (red curve).

Both plots show field gas in place increase when CO_2 is injected into the reservoir. However, when Sgc = 0.15 we have the higher amount of FGIP, This difference is a result of gas trapping mechanisms. When we set a value for Sgc, the gas cannot flow until pass this value, so the CO2 remain into the reservoir and trapped, while in the case without Sgc, the gas be able to flow as soon as injected into the reservoir.

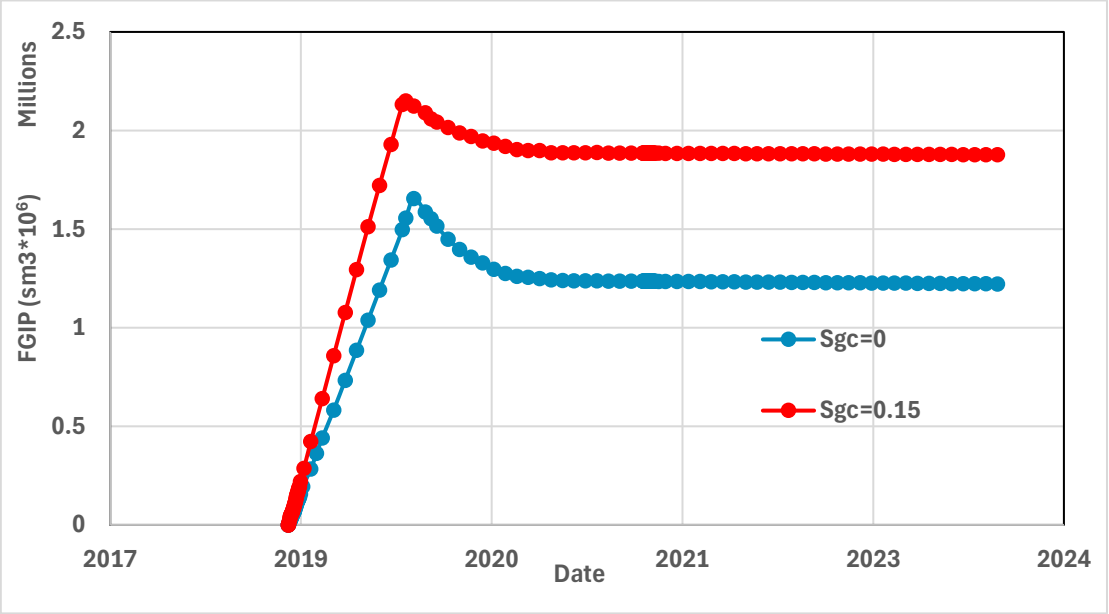

Figure 27 Field Gas In Place (FGIP) in Sm³ vs Date for Sgc=0 and Sgc=.015

IV. Comparison of CO_2 Injection Modeling via CO2STORE in OPM vs. tNavigator

The CO2STORE keyword in both OPM and tNavigator activates simulation features specifically designed for modeling CO_2 storage in deep saline aquifers. It enables the representation of key physical and chemical processes such as multiphase flow of CO_2 and brine, thermodynamic behavior of CO_2 under reservoir conditions, and CO_2 dissolution into formation water.

This keyword configures the simulator to handle high-pressure, high-temperature conditions typical of geological storage, including supercritical CO_2 injection, density and viscosity variation, and relative permeability effects. In tNavigator, it can also enable advanced features like geomechanical coupling and ionic effects on solubility. Overall, CO2STORE serves as a critical switch that tailors the simulator for realistic and accurate modeling of carbon capture and storage (CCS) scenarios.

1. CO2STORE in OPM

OPM implements the CO2STORE option in its flow simulator to model non-isothermal, multiphase flow of CO_2 and brine in porous media and designed to reflect the long-term behavior of CO_2 in deep saline aquifers.

The key features of this model are:

- Equation of State: Uses the Span-Wagner EOS for pure CO_2, providing accurate thermodynamic data over a wide temperature and pressure range.[36]
- Brine Modeling: Water phase properties (density, viscosity) depend on temperature and pressure; salinity can be included.
- CO_2 Dissolution: Supports convective dissolution of CO_2 into brine (solubility trapping).
- Heat Transport: Can include temperature effects to simulate thermal injection scenarios.
- Numerical Methods: Based on fully implicit formulation and finite-volume discretization

The CO2-Brine PVT model in OPM computes the PVT properties such as density, viscosity, and enthalpy internally by using analytic correlations and models from the literature instead of by interpolation from tabulated values. Table 5 presents the references for CO_2–brine properties used in OPM.

Property	Phase / Component	Reference
Density	Brine / Water	Hu et al. [38]; Wagner & Pruß [39]
	Dissolved CO_2	Garcia [40]
	CO_2	Span & Wagner [41]
Viscosity	Brine	Batzle & Wang [42]
	CO_2	Fenghour et al. [43]
Solubility	—	Spycher et al. [44]
Enthalpy	Brine / Water	Wagner & Kruse [45]
	Dissolved CO_2	Duan & Sun [46]
	CO_2	Span & Wagner [41]
Diffusivity	Water	McLachlan & Danckwerts[47]
Tortuosity	—	Millington & Quirk [48]
Salinity		Batzle & Wang [42]
		Ratcliff & Holdcroft [49]
		Daubert et al. [50]

Table 5 CO_2–brine properties references in OPM [37]

2. CO2STORE in tNavigator

In tNavigator, the CO2STORE keyword activates a dedicated module for simulating geological CO_2 storage, particularly in deep saline aquifers. This module integrates with the simulator's compositional framework, enabling accurate modeling of CO_2–brine interactions, including dissolution and salinity effects.

It also supports geomechanics coupling, letting users analyze caprock integrity and fault condition. Additionally, is used for uncertainty analysis, history matching, and evaluation different scenarios for CCS projects..

The key features of this model are:

- Equation of State: Supports CPA-SRK EOS for mixtures of CO_2, water, and salts whivh ideal for modeling CO_2 solubility in brine with ionic effects. [51]
- Brine Modeling: The software allows the use of different coefficient models to consider the influence of salts on CO_2 dissolution in water. This plays an important role for simulation the salting effect, where increasing salinity reduces the solubility of CO_2.
- CO_2 Dissolution: Includes solubility models based on different fugacity, temperature, and pressure .
- Numerical Methods:The method uses finite volumes combined with finite differences

to handle equations. It uses a fully implicit or adaptive implicit time approach. For heat flow, tNavigator includes the ROCKTABH feature, which helps model how rocks compress and expand in cycles of heating and cooling, affecting how easily fluids move in the reservoir.

In this thesis , we compare the result of both OPM and tNavigator in simulating CO_2 injection into saline aquifers using the CO2STORE keyword. As said before, OPM uses the Span-Wagner EOS and models for convective CO_2 dissolution with thermal effects. In contrast, tNavigator provides CPA-SRK EOS, geomechanical coupling, and advanced solubility modeling considering ionic interactions. While OPM excels in computational efficiency and transparency, tNavigator stands out for its compositional detail and user interface, making it more suited for complex industrial applications. Table 6 summarizes the CO2STORE keyword features in OPM and tNavigator.

Feature	OPM (CO2STORE)	tNavigator (CO2STORE)
EOS	Span-Wagner (pure CO_2)	CPA-SRK (CO_2 + brine + salts)
CO_2 Dissolution	Solubility via convective transport	Fugacity-based solubility with salt effects
Brine Properties	Pressure/temperature dependent	Fully compositional with salinity
Geomechanics	Not supported	Supported (optional module)
Thermal Modeling	Yes	Yes
Simulation Method	Fully implicit, finite-volume	Fully implicit, high-order solvers
Model type	Black-oil	Compositional
Geochemical interactions	Mineral dissolution Salt precipitation Coupling with MOOSE (the geochemistry module)	Integrated
3D visualization in time	ResInsight module	Integrated
Input/output	Standard industry formats (ex. Eclipse format) Vtk for Paraview visualization	Standard industry formats (ex. Eclipse format)
Scalability	Parallel mode	Parallel mode
Flexibility	Open source	no

Table 6 Compare CO2STORE keyword features in OPM and tNavigator

3. Comparison of Block Gas Saturation in Tnavigator and OPM

This section presents a comparison of the simulation results obtained using tNavigator and OPM for the reservoir model explained previously. Both simulations created using identical reservoir properties and injection parameters, which are summarized in Table 3. The goal is to check how consistent and effective the two simulators are over time when using the same model properties. The first thing measured is the gas saturation in three chosen grid blocks, which discussed earlier in the model description.

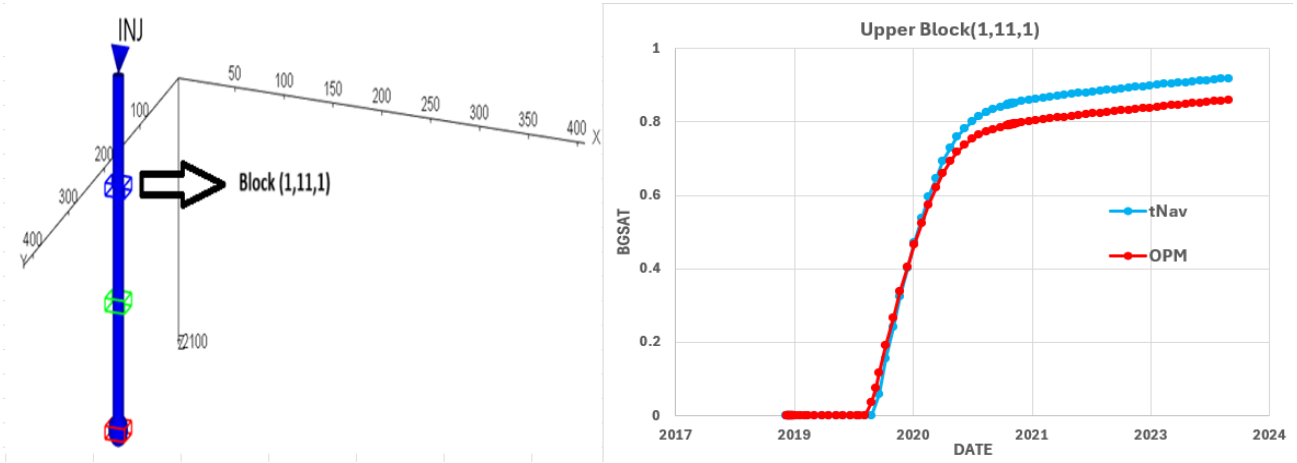

Figure 28 Block gas saturation vs Time for upper block (1,11,1)

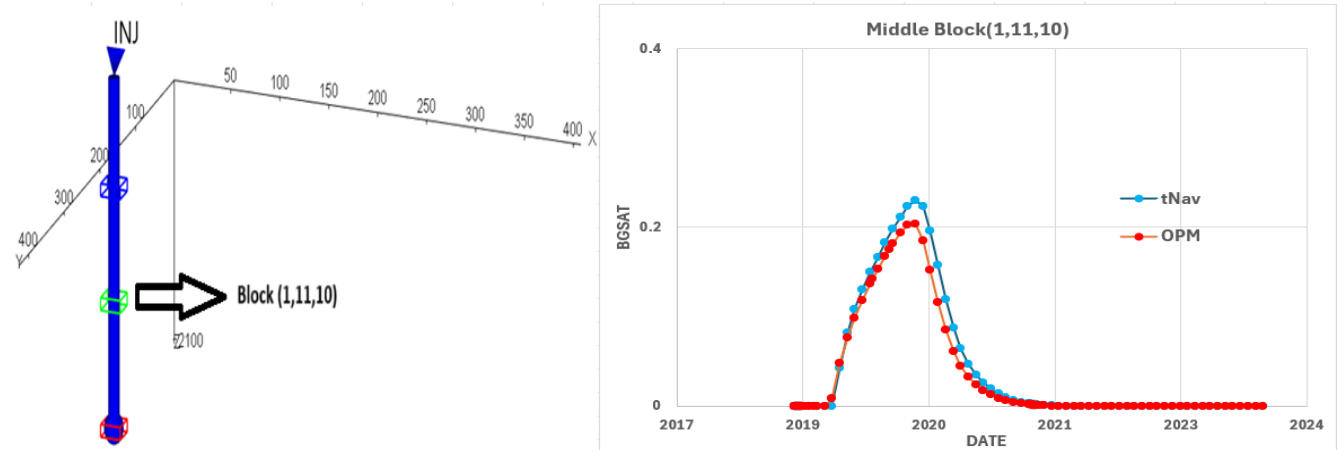

Figure 29 Block gas saturation vs Time for middle block (1,11,1)

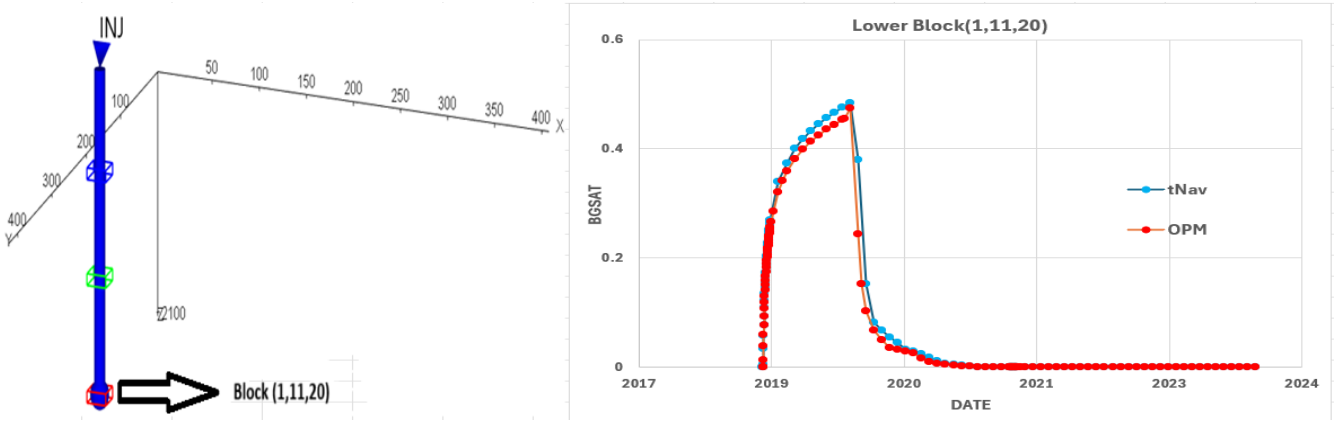

Figure 30 Block gas saturation vs Time for lower block (1,11,20)

4. Comparison of WBHP and WBP in tNavigator and OPM

Figure 32 illustrates the comparison of pressure profiles from both simulators. The left plot shows the Well Bottom Hole Pressure (WBHP) and the right plot provides the Well Bottom Pressure (WBP) during the injection phase in the same time.

The injection starts from early 2019 to mid 2021, during which gas is injected at controlled rates into the reservoir. Both tNavigator and OPM show consistent pressure behavior during this phase.

The data points from Tnavigator (blue) and OPM (red) match very closely, showing that both simulators give almost the same results for wellbore pressure with the same inputs. This agreement means that both programs manage well control and fluid flow in a similar way for this case.

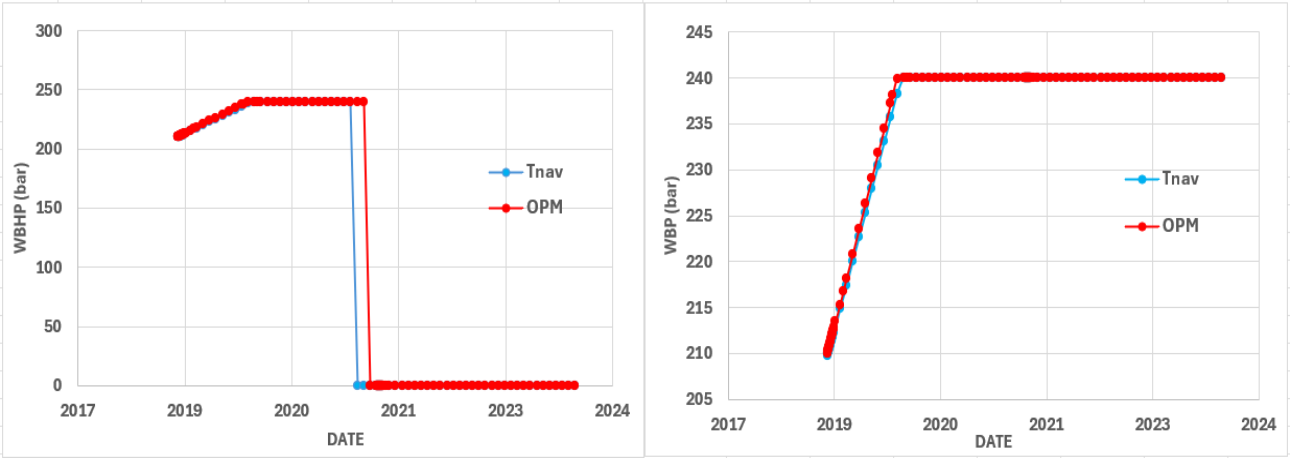

Figure 31 well bottom hole pressure (WBHP-left plot) and well bottom pressure (WBP-right plot) vs Date.

5. Comparison of WGIT and WGIR in tNavigator and OPM:

Figures 33 and 34 compare gas injection rate and total gas injection results in tNavigator and OPM in the same time of simulation.

As we can see in the graphs, both simulators show identical trends in gas injection behavior. The injection rate remains constant during the injection phase and then declines to near zero, and there is no significant deviation between the two software outputs. Similarly, the total gas injected follows the same trend in both simulators

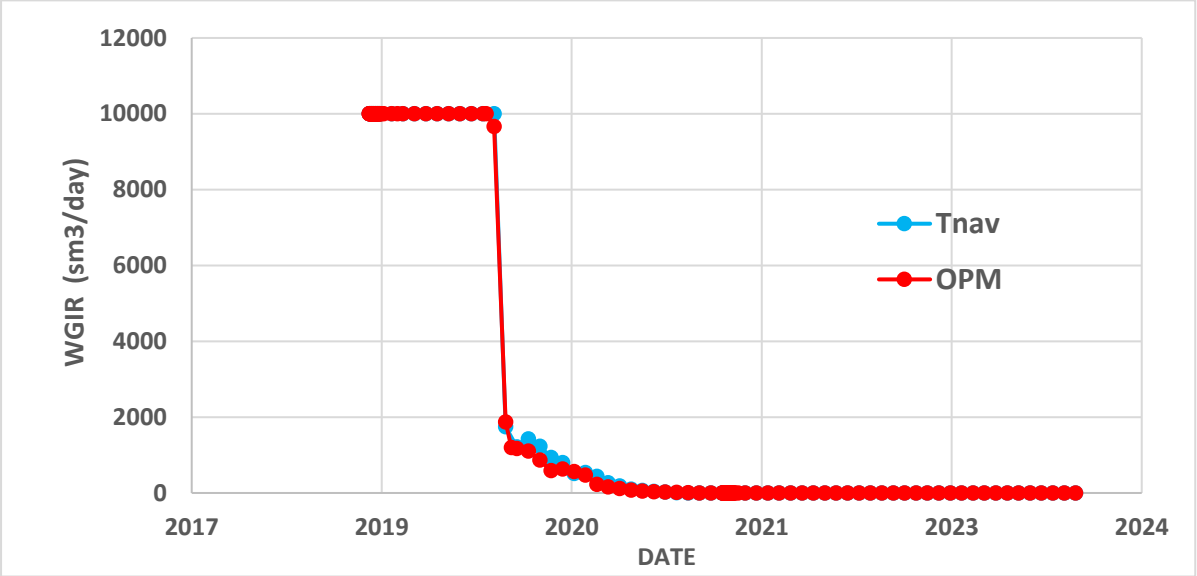

Figure 32 Gas injection rate (WGIR) in Sm³/day vs Date in Tnav (blue) and OPM (red)

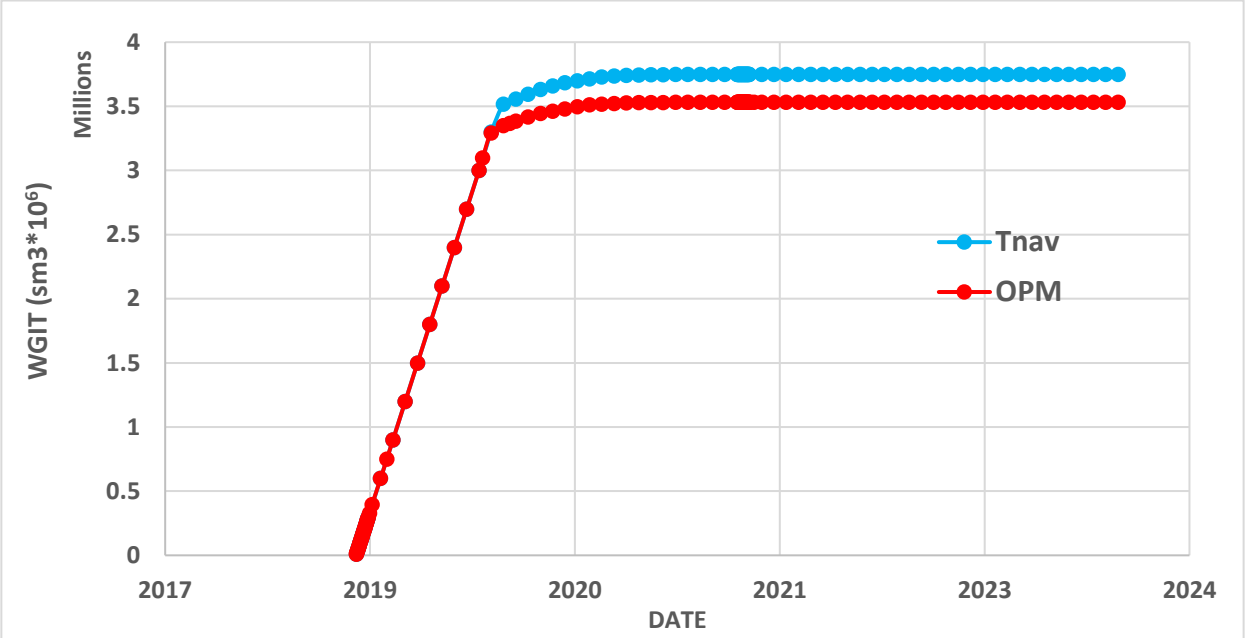

Figure 33 Total gas injection (WGIT) in Sm³ vs Date in Tnav (blue) and OPM (red)

6. Comparison of FGIP in TNavigator and OPM:

Figure 35 illustrates the Field Gas in Place (FGIP) over time, as simulated by tNavigator and OPM. The gas in place is presented in standard cubic meters (Sm³), and both simulators were run under identical reservoir and operational conditions.

As shown in the figure, While tNavigator (blue) shows slightly higher gas volumes compared to OPM (red)—particularly after the peak—the overall behavior and trajectory are highly consistent across both simulators. The differences are minor and can be attributed to variations in numerical solvers, grid handling, or interpolation schemes.

In summary, both simulators predict very similar field gas in place profiles, indicating a strong agreement in reservoir behavior modeling under the same input conditions.

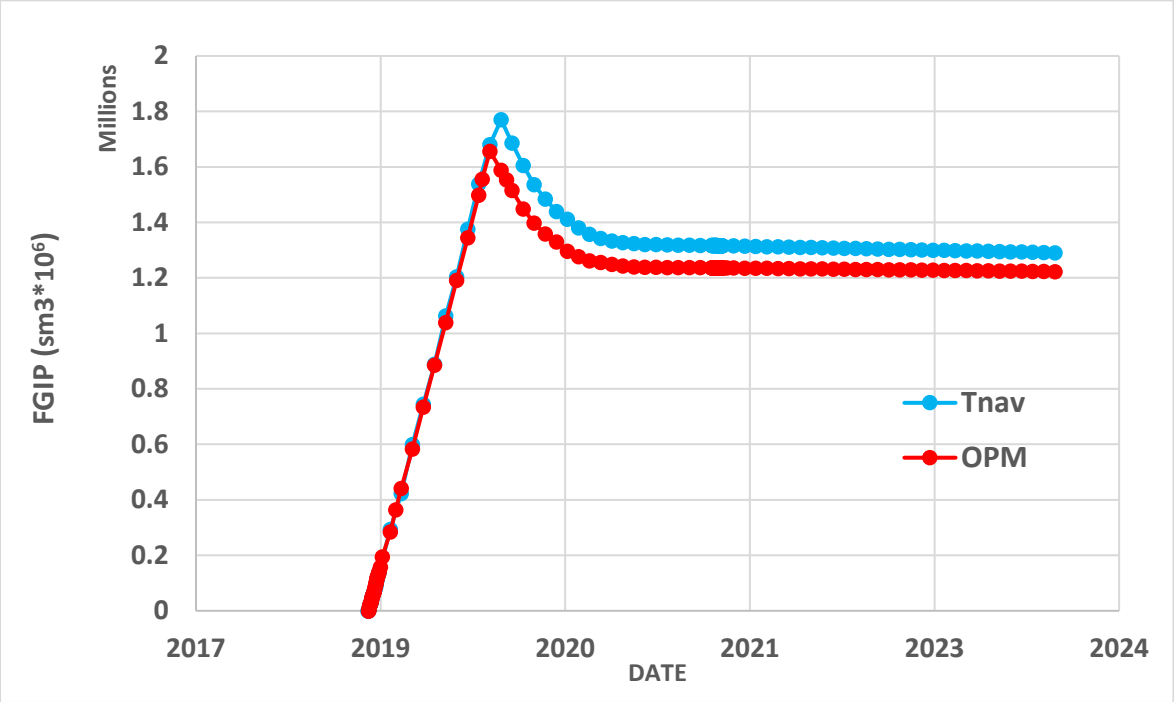

Figure 34 Field Gas In Place (FGIP) in Sm³ vs Date for tNav and OPM

7. Changing Kr exponent in OPM:

In general, one should not enter laboratory derived relative permeability data directly into the simulator. This is because it is dubious that laboratory measurements on 1½ inch core plugs can represent the flow in 100 x 100 x 1.0 m grid cell in the model. There are various upscaling techniques that can account for the scaling issue, using various forms of relative permeability curves, including the laboratory curves, piston-like curves and thickness average curves etc. However, the resulting pseudo relative permeability curves tend to not have smooth derivatives, which will have a detrimental impact on convergence efficiency. Thus, it is common practice to use the laboratory derived curves, either in an upscaling workflow or as part of the input workflow, and to fit a Corey type curve to the "rock" curves in order to smooth out any discontinuities.

Corey combined the work of Purcell and Burdine that was widely accepted for its simplicity. His original equations were developed for the drainage cycle in water-wet sandstones, but have also been used in carbonate formations. Corey's original water-oil equations were as follows:

$$K_{ro}(S_w) = \left[\frac{1 - S_w}{1 - S_{wcr}}\right]^{n_o}$$

$$K_{rw}(S_w) = \left[\frac{S_w - S_{wcr}}{1 - S_{wcr}}\right]^{n_w}$$

Where:

$K_{ro}(S_w)$ = relative permeability to oil,

$K_{rw}(S_w)$ = relative permeability to water

n_o = Corey oil exponent

n_w = Corey water exponent

S_w = water saturation,

S_{wcr} = critical water saturation.

The denominator in above equations scales the water saturation to the mobile water phase. There are several forms of these equations, with the most common normalizing the saturation over the mobile hydrocarbon phase, as depicted in below equations:

$$K_{ro}(S_w) = K_{row}\left[\frac{1 - S_w - S_{orw}}{1 - S_{orw} - S_{wcr}}\right]^{n_o}$$

$$K_{rw}(S_w) = K_{rww}\left[\frac{S_w - S_{wc}}{1 - S_{orw} - S_{wcr}}\right]^{n_w}$$

Where:

K_{row} = maximum oil relative permeability at Swc

K_{rw} = maximum water relative permeability st Sorw

S_{wc} = critical water saturation,

S_{orw} = residual oil saturation under a water flood (SOWCR)

Similar equations exist for gas-oil and water-oil systems. As mentioned above, the denominator in the equations, normalizes the saturation to the mobile phase, as a consequence, it is still necessary to extend the resulting Corey water curve to 100% water saturation in order to correctly model the water leg.

In this section, we modify the oil and gas exponent ng=no=2 (in OPM, water is modeled using the oil phase, as previously noted) to better observe the block gas saturation (In the base case, only two points were considered, means ng=no=1). Additionally, we assume zero critical gas saturation and residual oil saturation, and use the Corey correlation to calculate relative permeability for each gas saturation value. The results are illustrated in Figures 36 through 38 for the three selected grid blocks.

In the case where ng=no=2, the relative permeability curves become more concave, leading to reduced relative permeability values for both gas and water. As a result, the gas mobility decreases, causing the gas front to advance more slowly compared to the base case.

This behavior is clearly observed in the upper block (1,11,1) (Figure 36), where the base case exhibits significantly higher gas saturation due to the faster upward movement of gas. on the other hand , when we set ng = no = 2 ,the movement of the gas become slower and as a result we see lower saturation in the upper section of the column.

However, in the middle and lower blocks (Figures 37 and 38), because gas moves in the upper part slower, the saturation in deeper blocks is higher. As a result, gas saturation in the

ng = no=2 case is higher than in the base case, particularly in the middle block, where gas

concentration increases and then gradually decreases over time.

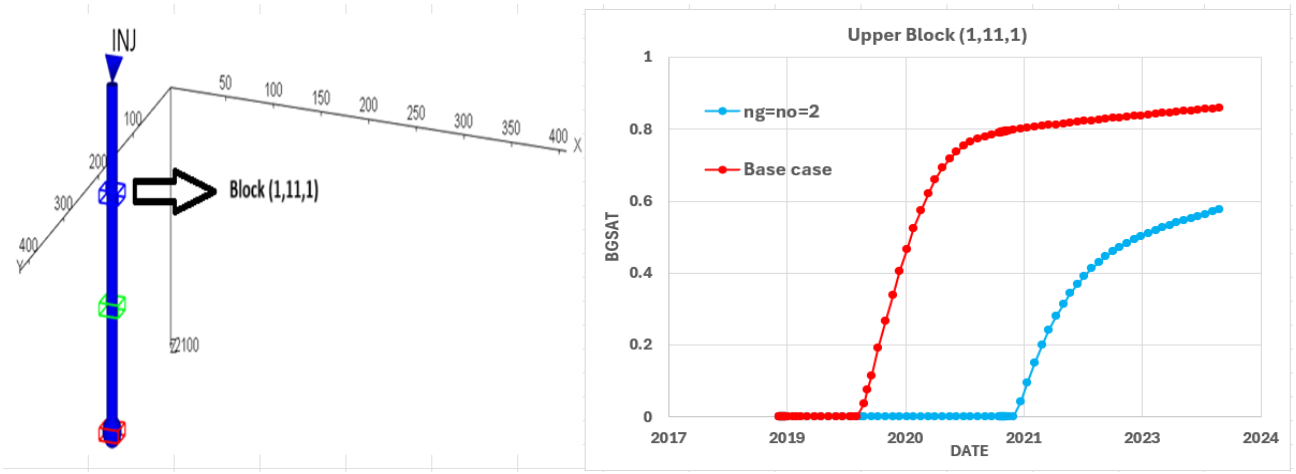

Figure 35 Block gas saturation vs Time for upper block (1,11,1) for ng=no=2 and base case.

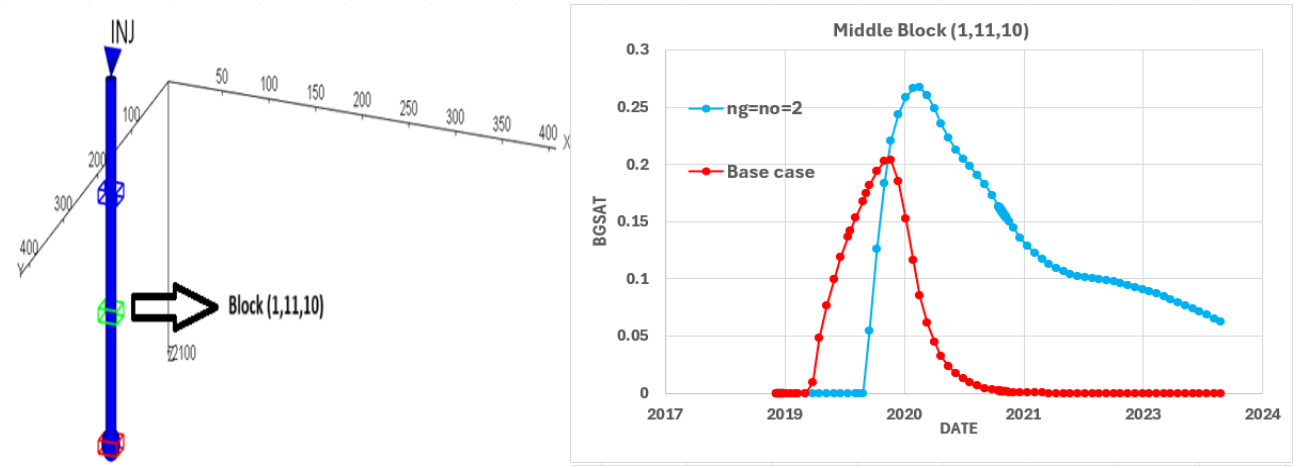

Figure 36 Block gas saturation vs Time for middle block (1,11,10) for ng=no=2 and base case.

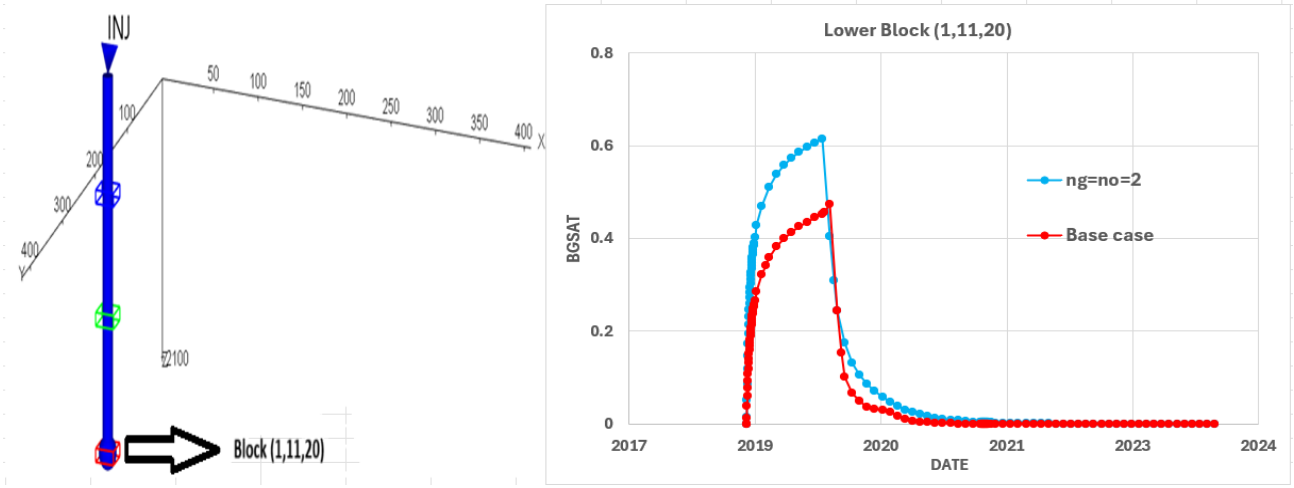

Figure 37 Block gas saturation vs Time for lower block (1,11,20) for ng=no=2 and base case.

8. Dissolution (DISS) vs. Diffusion (DIFF) in CO_2–Brine Systems in OPM:

We have two concepts In CO_2 storage simulations, dissolution and diffusion. the first one refers to the thermodynamic process that CO_2 dissolves into the brine phase. Pressure, temperature, and salinity mainly control this process. Dissolution determines the amount of CO_2 that can enter the brine under specific reservoir conditions.

By contrast, molecular diffusion describes the physical movement of dissolved CO_2 within the brine, where molecules spread from areas of higher concentration to lower concentration. This process follows Fick's Law, and need a long time to see its effect in CO2 injection simulation.

In the final part of the study, we analyse the results in two different model condition: one in which only dissolution (DISS) occurs, and another where both dissolution and diffusion (DISS+DIFF) are active. The outcomes of these scenarios are shown in Figures 39 through 43.

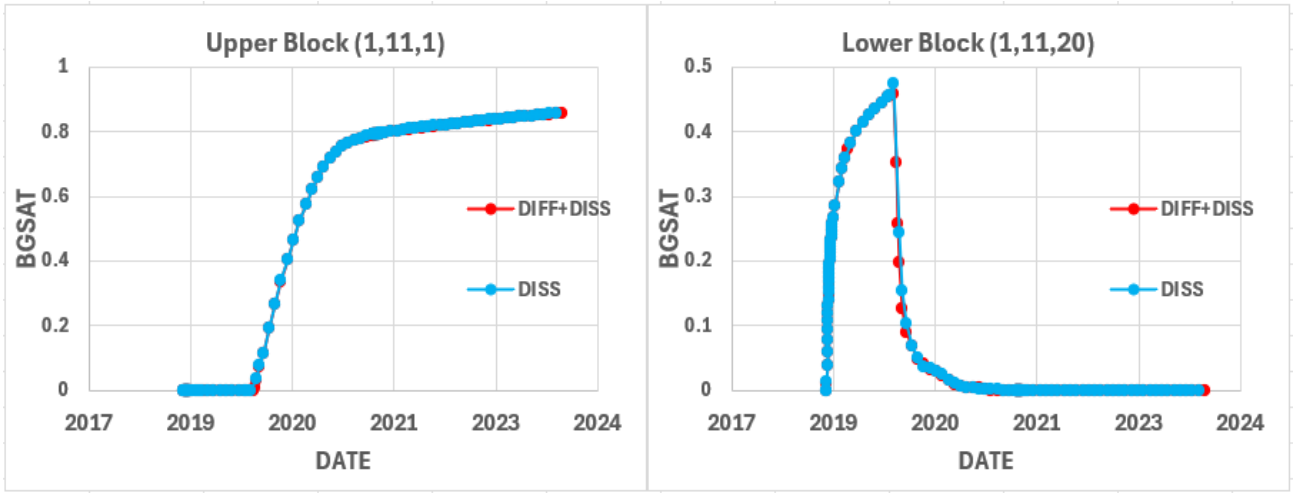

Figure 38 Block gas saturation vs Time for upper and lower block in dissolution and diffusion

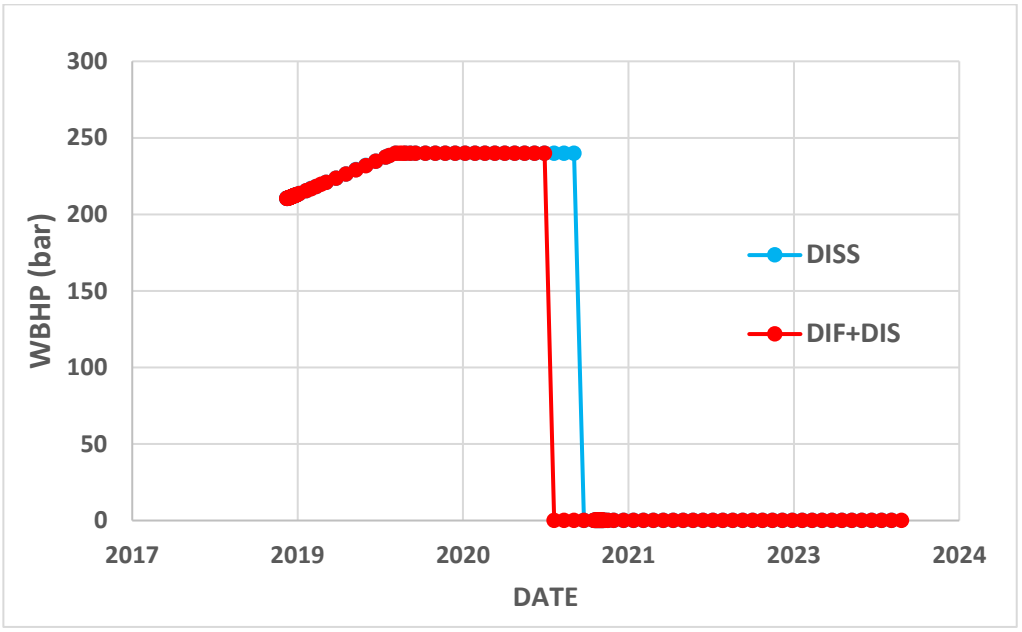

Figure 39 Well bottom hole pressure vs Time in dissolution and diffusion

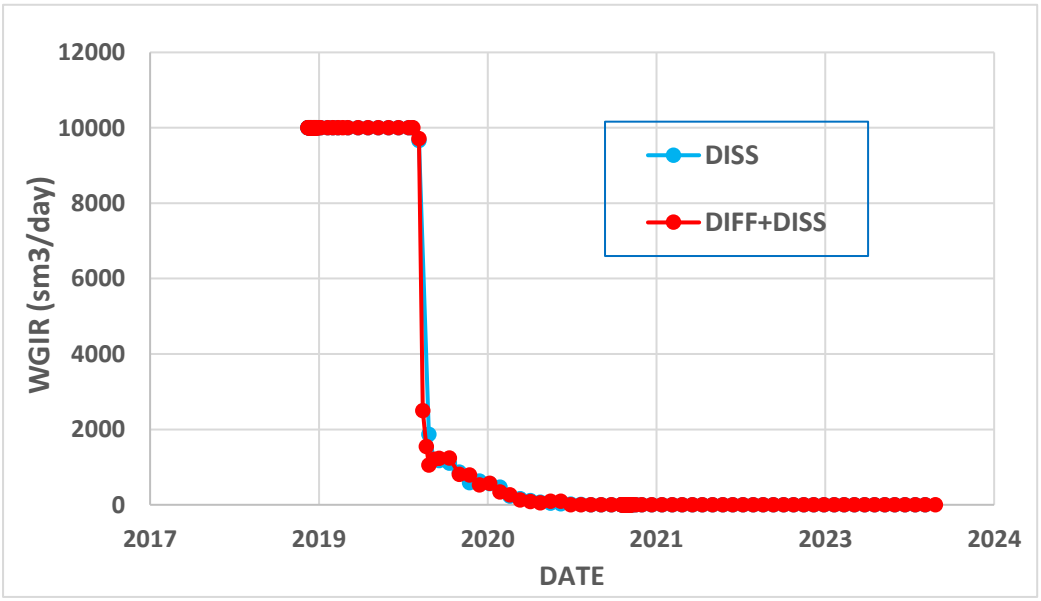

Figure 40 Well gas injection rate vs Time in dissolution and diffusion

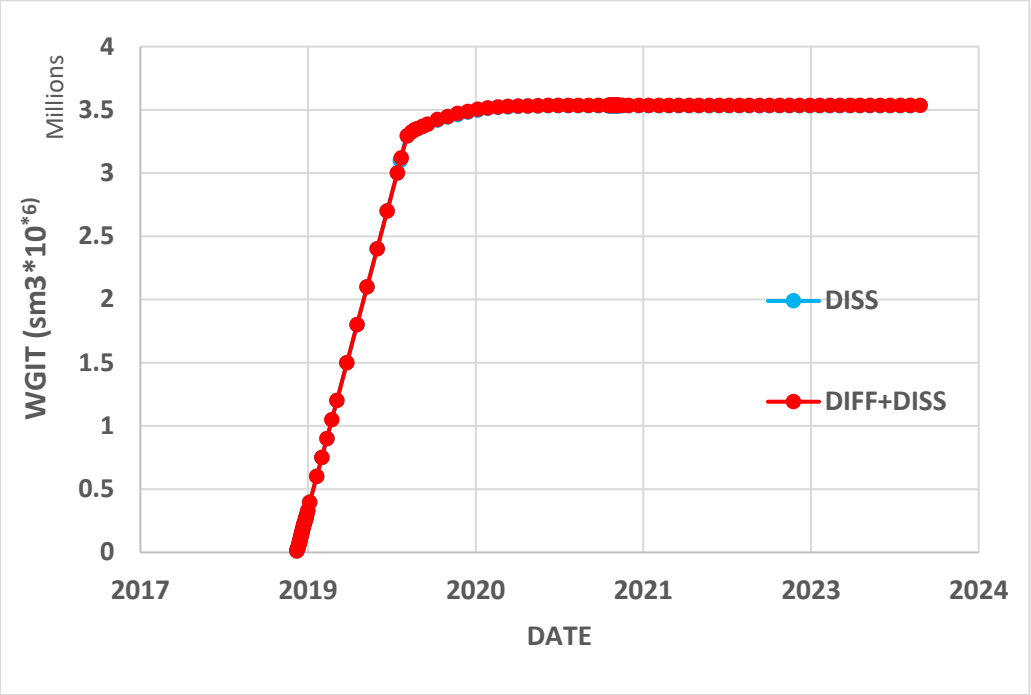

Figure 41 Well gas injection total vs Time in dissolution and diffusion

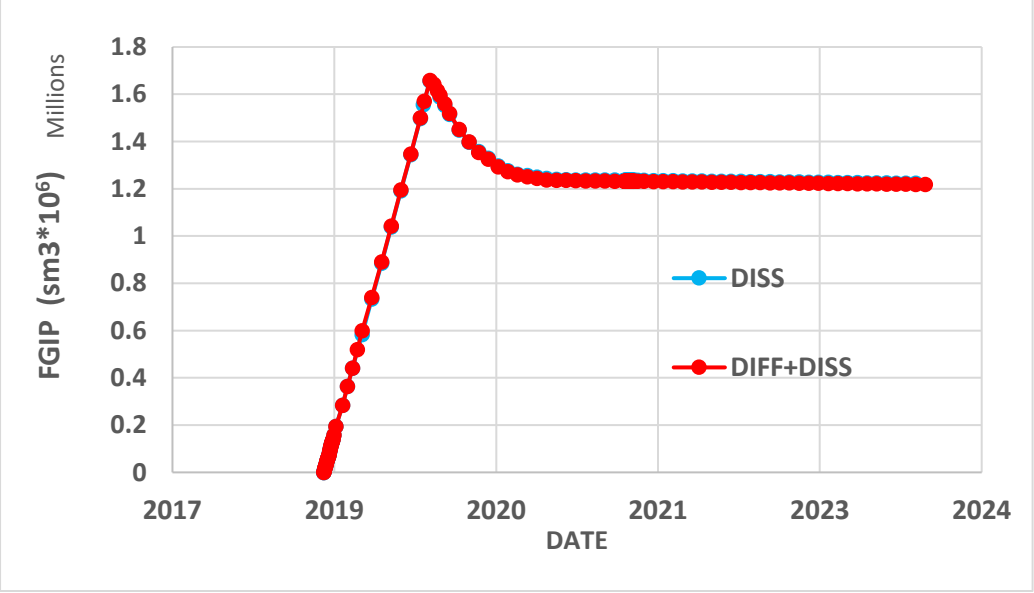

Figure 42 Field gas in place vs Time in dissolution and diffusion

As observed in the results, the inclusion of diffusion has a relatively minor impact on the properties examined in this study. While diffusion contributes to the gradual redistribution of dissolved CO_2 within the brine, its overall effect on key system parameters—such as pressure, gas saturation, and CO_2 concentration profiles—remains limited when compared to the dominant role of dissolution. This suggests that, under the conditions modeled, diffusion plays a secondary role in influencing the overall behavior of the CO_2–brine system.

V. Conclusion

This study presents a evaluation into the dynamic behavior of CO_2 injection and storage in underground porous media, with a particular focus on saline aquifers reservoirs. In this work, both OPM and tNavigator were used alongside to simulate how CO_2 behaves in underground storage systems. , the study provides valuable insights into the key parameters that influence the efficiency, and long term performance of geological CO_2 storage.

We did sensitivity analysis to see the effects of important factors such as reservoir depth, permeability, critical gas saturation, relative permeability exponents, and injection constraints on our simulation model. The results showed the significant role of permeability and critical gas saturation in gas mobility and storage capacity. It was found that when we put a non zero value for critical gas saturation , gas tends to move more slowly and it causes the efficiency of injection decreased..

The thesis also analyzed the role of dissolution and molecular diffusion in the CO_2–brine system. While dissolution was found to play a substantial role in redistributing injected CO_2 and moderating pressure buildup, diffusion exhibited only a minor impact under the simulated conditions. This suggests that, for the types of formations and time scales considered, dissolution remains the dominant mechanism influencing subsurface CO_2 behavior.

In addition, comparing the results from OPM and tNavigator showed strong agreement in the main simulation outcomes, such as pressure profiles, gas saturation, total gas injection, and gas in place.

In conclusion, this study showed that to carry out a successful project, in this case CO2 injection, must pay attention to all effective parameters and test and compare different strategies with different simulation softwares. The findings serve as a useful foundation for future CCS projects, particularly in optimizing injection schemes and evaluating site suitability for long-term carbon sequestration. These insights contribute meaningfully to global efforts in reducing greenhouse gas emissions and combating climate change.

Appendix A: Input File of base model in OPM

This appendix includes the reservoir simulation input deck used for CO_2 injection modeling.

```
-------------------------------------------------------------------------------
RUNSPEC
-------------------------------------------------------------------------------
TITLE
   CO2STORE

DIMENS
20 21 20 /

EQLDIMS
/

TABDIMS
/

OIL
GAS
CO2STORE
DISGAS
--DIFFUSE
--THERMAL

METRIC

START
   1 'JAN' 2019 /

WELLDIMS
   1 10 1 1 /

UNIFIN
UNIFOUT

-------------------------------------------------------------------------------
GRID
-------------------------------------------------------------------------------

NOECHO

INIT
```

```
DX
  8400*20 /

DY
  8400*20 /

DZ
  8400*5 /

TOPS
  420*2000.0 /

PORO
  8400*0.3/

PERMX
  8400*2000/

PERMY
  8400*2000/

PERMZ
  8400*2000/
-------------------------------------------------------------------------------
PROPS
-------------------------------------------------------------------------------

ROCK
  1.0 1e-6 /

SGOF
0       0       1       0.0
1       1       0       0.0 /

SALINITY
 0.7/ 35-40g/l  -> 35-40g /kg -> 0.63-0.72 mol/g
```

```
--------------------------------------------------------------------------------
SOLUTION
--------------------------------------------------------------------------------

EQUIL
 2000 200 2500 0 0 0 1 1 0 /

RTEMPVD
  0 50
  100 50
/

RSVD
  0 0.0
  100 0.0 /

RPTRST
 'BASIC=2' 'ALLPROPS'/

--------------------------------------------------------------------------------
SUMMARY
--------------------------------------------------------------------------------
WBHP
   'INJ'
   'PROD'
/

BGSAT
  1 11 1 /
  1 11 10 /
  1 11 20 /
/

BPR
  1 11 1 /
  1 11 10 /
  1 11 20 /
/
BRS
  1  11 1 /
  1  11 20/
/
FPR
/
FGIT
/
RUNSUM

DATE

--------------------------------------------------------------------------------
SCHEDULE
--------------------------------------------------------------------------------

RPTRST
 'BASIC=2' 'ALLPROPS'/

WELSPECS
-- Item #: 1     2      3       4       5        6
        'INJ'   'G1'    1       11      1*      'GAS' /
/
COMPDAT
-- Item #: 1    2       3       4       5       6       7       8       9
        'INJ'   1       11      20      20      'OPEN'  1*      1*      0.5 /
/

WCONINJE
-- Item #:1      2       3       4      5      6  7
        'INJ'   'GAS'   'OPEN'  'RATE'  1000  1*  250 /
/

-- 30 day
TSTEP
20*365
/
END
```

Appendix B: Input File of base model in tNavigator

This appendix includes the reservoir simulation input deck used for CO_2 injection modeling.

```
-----------------------------------------------------------------------------------------
RUNSPEC
-----------------------------------------------------------------------------------------
TITLE
   CO2STORE

METRIC

START
   1 'JAN' 2019 /

DIMENS
20 21 20 /


WATER
GAS
CO2STORE

COMPS
 2 /
UNIFIN
UNIFOUT

-----------------------------------------------------------------------------
GRID
-----------------------------------------------------------------------------------------

NOECHO

INIT

DX
  8400*20 /

DY
  8400*20 /

DZ
  8400*5 /
```

```
TOPS
  420*2000.0 /

PORO
  8400*0.3/

PERMX
  8400*500/

PERMY
  8400*500/

PERMZ
  8400*50/


-----------------------------------------------------------------------------------------------
PROPS
-----------------------------------------------------------------------------------------------
ROCK
  1.0 1e-6 /

COREYWG
-- SWL SWU SWCR SGWCR KRGU KRG    KRW  KRWU  PC  ng  nw
   0    1   0    0    1     1     1    1    0   1   1   *2  /


SALINITY
 0.7/ 35-40g/l  -> 35-40g /kg -> 0.63-0.72 mol/g

NCOMPS
 2 /

CNAMES
 'CO2' 'H2O'/

ZI
 -- composition
 0  1/
```

```
RTEMP
-- reservoir temperature
   50       /


-------------------------------------------------------------------------------
SOLUTION
-------------------------------------------------------------------------------

EQUIL
--depth pressure WOC   PCWO  GOC  PCGO
 2000     200    1500   0     0    0  /


RPTRST
 'BASIC=2' 'ALLPROPS'/

-------------------------------------------------------------------------------
SUMMARY
-------------------------------------------------------------------------------

WBHP
   'INJ'

/
WBP
/
WGIR
/
WGIT
/
FGIPG
/
BGSAT
  1 11 1 /
  1 11 10 /
  1 11 20 /
/
```

```
BPR
  1 11 1 /
  1 11 10 /
  1 11 20 /
/

BRS
  1  11 1 /
  1  11 20/
/
FPR
/
FGIT
/
RUNSUM

DATE

-------------------------------------------------------------------------------
SCHEDULE
-------------------------------------------------------------------------------


RPTRST
 'BASIC=2' 'ALLPROPS'/

WELSPECS
-- Item #: 1     2      3       4       5       6
        'INJ'   'G1'    1       11      1*      'GAS' /
/
COMPDAT
-- Item #: 1    2       3       4       5       6       7       8       9
        'INJ'   1       11      20      20      'OPEN'  1*      1*      0.5 /
/
```

```
WELLSTRE
-- stream_name  mole_fractions
 'INJGAS' 1 0  /
/

WINJGAS
-- wname   fluid_nature inj.stream mnemonic sep.stage
   'INJ' STREAM       'INJGAS'   /
/
-----------------------------------------------------------------------------------------------------------

WCONINJE
-- Item #:1      2       3       4      5      6  7
        'INJ'   'GAS'   'OPEN'  'RATE'  10000  1*  240 /
/

-- 30 day
TSTEP
30*1
/

TSTEP
30*30
/
WCONINJH
-- Item #:1      2       3
        'INJ'   'GAS'   'STOP'   /
/

TSTEP
30*1
/

TSTEP
30*30
/


END
```

BIBLIOGRAPHY

1. Miocic, J.M., G. Johnson, and C.E. Bond, *Uncertainty in fault seal parameters: implications for CO 2 column height retention and storage capacity in geological CO 2 storage projects.* Solid earth, 2019. **10**(3): p. 951–967.
2. Azpiroz, J.T., et al., *Optimizing carbon dioxide trapping for geological storage.* arXiv preprint arXiv:2312.13512, 2023.
3. Association, W.N. *Climate Change – The Science*. 2023; Available from: https://world-nuclear.org/information-library/energy-and-the-environment/climate-change-the-science.
4. Impact, W.s.Y. *Main Sources of Carbon Dioxide Emissions*. 2023; Available from: https://whatsyourimpact.org/greenhouse-gases/carbon-dioxide-emissions.
5. Marzouk, O.A. *Summary of the 2023 Report of TCEP (Tracking Clean Energy Progress) by the International Energy Agency (IEA), and Proposed Process for Computing a Single Aggregate Rating*. in *E3S Web of Conferences*. 2025. EDP Sciences.
6. Metz, B., et al., *IPCC special report on carbon dioxide capture and storage*. 2005: Cambridge: Cambridge University Press.
7. Climate.gov, N. *Global Carbon Dioxide Emissions and Atmospheric Carbon Dioxide (1751–2024)*. 2024; Available from: https://www.climate.gov.
8. Loh, P.M., et al., *Estimating Atmospheric Forest Carbon Loss in East Baton Rouge Parish Using Satellite Remote Sensing: A Critical Tool for Climate Change Mitigation.* The International Archives of the Photogrammetry, Remote Sensing and Spatial Information Sciences, 2025. **48**: p. 101–107.
9. (UNFCCC), U.N.F.C.o.C.C. *Adoption of the Paris Agreement*. 2015; Available from: https://unfccc.int/process-and-meetings/the-paris-agreement.
10. Lipponen, J., *Carbon Capture and Storage-Progress and Next Steps.* 2010.
11. O'Brien, K.C., *Center for Utilization of Captured CO2 (CUC-CO2) Creating a Market for Captured CO2*. 2016, University of Illinois, Office of Business and Financial Services, 1901 ….
12. Kobakhidze, N. and R. Balasubramanian, *Carbon capture, utilization, and storage activities and sustainability reporting by oil and gas companies*. 2023, University of South-Eastern Norway.
13. Jenkins, L.T., M. Foschi, and C.W. MacMinn, *Impact of pressure dissipation on fluid injection into layered aquifers.* Journal of Fluid Mechanics, 2019. **877**: p. 214–238.
14. Lokhorst, A. and T. Wildenborg, *Introduction on CO2 Geological storage-classification of storage options.* Oil & gas science and technology, 2005. **60**(3): p. 513–515.
15. Lal, R., *Soil carbon sequestration impacts on global climate change and food security.* science, 2004. **304**(5677): p. 1623–1627.
16. Wei, B., et al., *CO2 storage in depleted oil and gas reservoirs: A review.* Advances in Geo-Energy Research, 2023. **9**(2): p. 76–93.
17. Lockwood, T. and T. Bertels, *A European Strategy for Carbon Capture and Storage*. 2022, Tech. Rep., Clean Air Task Force (CAFT).
18. Benson, S.M. and D.R. Cole, *CO2 sequestration in deep sedimentary formations.* Elements, 2008. **4**(5): p. 325–331.
19. Bentham, M. and M. Kirby, *CO2 storage in saline aquifers.* Oil & gas science and technology, 2005. **60**(3): p. 559–567.
20. Rodrigues, C.F., et al., *Developments and Evolution of CCUS Technologies: A Review.* Carbon Capture Utilization and Storage: Law, Policy and Standardization Perspectives, 2025: p. 35–85.
21. Metz, B., *Carbon dioxide capture and storage: special report of the intergovernmental panel on climate change*. 2005: Cambridge University Press.
22. Rubin, E. and H. De Coninck, *IPCC special report on carbon dioxide capture and storage.* UK: Cambridge University Press. TNO (2004): Cost Curves for CO2 Storage, Part, 2005. **2**: p. 14.
23. Wipki, M., et al. *CO2CARE-Site Closure Assessment Research-Recent Results*. in *EGU General Assembly Conference Abstracts*. 2013.
24. Solomon, S., et al., *A proposal of regulatory framework for carbon dioxide storage in geological formations.* International Risk Governance Council, 2007.
25. de Kleijne, K., et al., *Limits to Paris compatibility of CO2 capture and utilization.* One Earth, 2022. **5**(2): p. 168–185.
26. Solomon, S., *Criteria for intermediate storage of carbon dioxide in geological formations.* The Bellona Foundation, Oslo, 2006: p. 1–6.

27. Corporation, C., *CO_2 Phase Diagram. Drawn with CO_2 Tab V1.0*. 1999, Retrieved from: https://www.chemicalogic.com.
28. Srl, U. *What Happens to Fluid Properties Near the Critical Point?* 2023 Available from: https://www.unilab.eu/articles/fluid-properties-near-critical-point/.
29. (USGS), U.S.G.S. *Example 22 – CO_2 Solubility at High Pressure (25–100 °C)*. n.d; Available from: https://water.usgs.gov/water-resources/software/PHREEQC/documentation/phreeqc3-html/phreeqc3-84.htm.
30. Tsar, M., M. Ghasemiziarhani, and K. Ofori. *The effect of well orientation (vertical vs. horizontal) on co2 sequestration in a water saturated formation-saline aquifer in western australia*. in *SPE Europec featured at EAGE Conference and Exhibition?* 2013. SPE.
31. Jiang, X., *A review of physical modelling and numerical simulation of long-term geological storage of CO2.* Elsevier, November 2011.
32. Temitope Ajayi, J.S.G.A.B., *A review of CO2 storage in geological formations emphasizing modeling, monitoring and capacity estimation approaches.* Petroleum Science, 2019. **Volume 16, pages 1028–1063, (2019)**.
33. Urych, T., et al., *Numerical simulations of carbon dioxide storage in selected geological structures in north-western Poland.* Frontiers in Energy Research, 2022. **10**: p. 827794.
34. Rasmussen, A.F., et al., *The open porous media flow reservoir simulator.* Computers & Mathematics with Applications, 2021. **81**: p. 159–185.
35. Todd, M. and W. Longstaff, *The development, testing, and application of a numerical simulator for predicting miscible flood performance.* Journal of Petroleum Technology, 1972. **24**(07): p. 874–882.
36. OPM-OP AS Oscars Gate 27, O., Norway since 2023: Matthew Goodfield, 2017-2023 David Baxendale and *OPM_Flow_Reference_Manual_2023-10_Rev-0.fodt*. 2023–10.
37. Sandve, T.H., et al. *Convective dissolution in field scale CO2 storage simulations using the OPM flow simulator*. in *TCCS–11. CO2 capture, transport and storage. Trondheim 22nd–23rd June 2021 short papers from the 11th international Trondheim CCS conference*. 2021. SINTEF Academic Press.
38. Hu, J., et al., *PVTx properties of the CO2–H2O and CO2–H2O–NaCl systems below 647 K: Assessment of experimental data and thermodynamic models.* Chemical Geology, 2007. **238**(3-4): p. 249–267.
39. Wagner, W. and A. Pruß, *The IAPWS formulation 1995 for the thermodynamic properties of ordinary water substance for general and scientific use.* Journal of physical and chemical reference data, 2002. **31**(2): p. 387–535.
40. Garcia, J.E., *Density of aqueous solutions of CO2.* 2001.
41. Span, R. and W. Wagner, *A new equation of state for carbon dioxide covering the fluid region from the triple-point temperature to 1100 K at pressures up to 800 MPa.* Journal of physical and chemical reference data, 1996. **25**(6): p. 1509–1596.
42. Batzle, M. and Z. Wang, *Seismic properties of pore fluids.* Geophysics, 1992. **57**(11): p. 1396–1408.
43. Fenghour, A., W.A. Wakeham, and V. Vesovic, *The viscosity of carbon dioxide.* Journal of physical and chemical reference data, 1998. **27**(1): p. 31–44.
44. Spycher, N., K. Pruess, and J. Ennis-King, *CO_2-H_2O mixtures in the geologic sequestration of CO_2. I. Assessment and calculation of mutual solubilities from 12 to 100 degrees C and up to 600 bar.* Geochimica et Cosmochimica Acta, 2002. **67**(LBNL-50991).
45. Wagner, W. and A. Kruse, *Properties of water and steam: the industrial standard IAPWS-IF97 for the thermodynamic properties and supplementary equations for other properties: tables based on these equations= Zustandsgrössen von Wasser und Wasserdampf: der Industrie-Standard IAPW-IF97 für die thermodynamischen Zustandsgrössen und ergänzende Gleichungen für andere Eigenschaften: Tafeln auf der Grundlage dieser Gleichungen.* (No Title), 1998.
46. Duan, Z. and R. Sun, *An improved model calculating CO2 solubility in pure water and aqueous NaCl solutions from 273 to 533 K and from 0 to 2000 bar.* Chemical geology, 2003. **193**(3-4): p. 257–271.
47. McLachlan, C. and P. Danckwerts, *Desorption of carbon dioxide from aqueous potash solutions with and without the addition of arsenite as a catalyst.* Trans. Inst. Chem. Eng, 1972. **50**: p. 300–309.
48. Millington, R. and J. Quirk, *Permeability of porous solids.* Transactions of the Faraday Society, 1961. **57**: p. 1200–1207.
49. Ratcliff, G. and J. Holdcroft, *Diffusivities of gases in aqueous electrolyte solutions.* Trans. Inst. Chem. Eng, 1963. **41**(10): p. 315–319.
50. Daubert, T.E., *Physical and thermodynamic properties of pure chemicals: data compilation.* Design Institute for Physacal Property Data (DIPPR), 1989.
51. Spycher, N. and K. Pruess, *CO2-H2O mixtures in the geological sequestration of CO2. II. Partitioning in chloride brines at 12–100 C and up to 600 bar.* Geochimica et Cosmochimica acta, 2005. **69**(13): p. 3309–3320.